

# Controller Design and Analysis for Elevator Failure in the F-4 and Learjet-25

Layne Aure, Carissa Castellano, Jacob Hansen, Nate Jacobs, Kaylee Patterson, Tiger Sievers\*, Paige Ward †, Ethan Wegner

This report presents the development of linear models for the Learjet 25 and the F-4 Phantom and a nonlinear model for the F-4. These models were verified using doublet responses and bode plots. The models were then used to construct flight controllers for the two aircraft and a simulator for the F-4. The information used to create the models for these aircraft was gathered from a variety of different sources detailing their flight characteristics in different flight configurations. This information, the models, the controllers and external literature will then be used to conduct an analysis of elevator failure across both aircraft, its effect on flight performance, and if possible, how the aircraft can compensate for the control surface failure using throttle input.

## I. Nomenclature

### A. Variables

$\mathbf{A}, \mathbf{B}, \mathbf{C}, \mathbf{D}$	= state-space matrices
$A$	= amplitude of oscillation
$c_{L_\alpha}$	= example of non-dimensional stability derivative, $C_{L_\alpha} \equiv \partial C_L / \partial \alpha$
$c_{L_{\delta_e}}$	= example of non-dimensional stability derivative, $C_{\delta_e} \equiv \partial C_L / \partial \delta_e$
$\bar{c}$	= chord
$c_\phi$	= example of short notation for trigonometry function of an angle
$\Delta t$	= time step
$F_x, F_y, F_z$	= total x-,y-,z-body axis force, lb
$f_x, f_y, f_z$	= perturbation x-,y-,z-body axis force, lb
$f, g$	= generic functions
$g$	= acceleration due to gravity, $ft/s^2$
$h$	= height, ft
$I$	= moment of inertia, $sl \cdot ft^2$
$K_p, K_i, K_d$	= controller gains for the proportional, integral, and derivative
$L, M, N$	= total roll, pitch, yaw moments ft-lb
$M_q$	= example of dimensional stability derivative $M_q \equiv (\partial M / \partial q) / I_{yy}$
$M_{\delta_e}$	= example of dimensional control derivative, $M_{\delta_e} \equiv (\partial M / \partial \delta_e) / I_{yy}$
$l, m, n$	= perturbation roll, pitch, yaw moments ft-lb
$m$	= mass, sl
$P, Q, R$	= Total roll, pitch, yaw rates, rad/s or deg/s
$P_N, P_E, P_D$	= Position in north, east and down direction, ft
$p, q, r$	= perturbation roll, pitch, yaw rates rad/s or deg/s
$\bar{q}$	= dynamic pressure, $lb/ft^2$
$S$	= platform area, $ft^2$
$t$	= time, s
$U, V, W$	= total x-,y-,z-body axis velocity, ft/s
$u, v, w$	= perturbation x-,y-,z-body axis velocity ft/s
$u$	= system input

---

\*Team Lead

†Report Lead

$V_B$	= total velocity in body coordinate system
$\alpha$	= angle of attack, rad or deg
$\beta$	= sideslip angle, rad or deg
$\delta$	= control deflection, rad or deg
$\Phi, \Theta, \Psi$	= total roll, pitch, yaw Euler angles, rad or deg
$\phi, \theta, \psi$	= perturbation roll, pitch, yaw Euler angles, rad or deg

## B. Subscripts

$A$	= aerodynamic force
$T$	= thrust
$a$	= aileron
$e$	= elevator
$h$	= horizontal stabilizer
$r$	= rudder
$1$	= trim state

## II. Introduction

THE use of digital flight controls for aircraft has spurred the development of digital aircraft simulators and digital twin flight controls that offer an opportunity to model and develop the control responses of the aircraft well before it takes flight. This methodology has allowed designers to save money and time in their development programs.

This advancement has not been seen quite as much in existing aircraft models however, already existing flight test data has been cheaper to upkeep and maintain than developing brand new digital models, but an increasing number of aircraft have begun to receive digital twins time goes on. A primary reason for this is developing for failure of flight control systems, where testing incurs a real risk of complete loss of the airframe.

To this end, system identification of the Learjet 25 and the F-4 Phantom was undertaken by a team from the University of Kansas as a part of a department wide project to develop flight control models for aircraft. The project developed linear models for the two aircraft, in both lateral and longitudinal aspects. These models were validated by doublet responses and frequency analysis. After validation, These models were then used to develop flight control software for both aircraft. Furthermore, the linear model for the F-4 Phantom was used to develop a nonlinear flight model. Then an analysis was performed using the models and information from to determine if thrust can compensate for elevator failure. This was done for both aircraft.



**Fig. 1 Aircraft Images**

### III. Theory

#### A. Non-linear system theory

A non-linear model of the F-4 was created to both compare to a linear F-4 model and analyze the behavior of a non-linear model. The model was created using the 12-state, 6-degree-of-freedom nonlinear equations of motion. These are seen in Equations 1 - 10 shown below. Equation 10 is presented using the notation used by Dr. Beard [1].

$$m(\dot{U} - VR + WQ) = -mgsin(\Theta) + F_x \quad (1)$$

$$m(\dot{V} + UR - WP) = mgsin(\Phi)cos(\Theta) + F_y \quad (2)$$

$$m(\dot{W} - UQ + VP = mgcos(\Phi)cos(\Theta) + F_z \quad (3)$$

$$I_{xx}\dot{P} - I_{xz}\dot{R} - I_{xz}PQ + (I_{zz} - I_{yy})RQ = L \quad (4)$$

$$I_{yy}\dot{Q} - (I_{xx} - I_{xz})PR + I_{xz}(P^2 - R^2) = M \quad (5)$$

$$I_{zz}\dot{R} - I_{xz}\dot{P} - I_{xz}QR + (I_{yy} - I_{zz})PQ = N \quad (6)$$

$$\dot{\Phi} = P + Qcos(\Phi)tan(\Theta) + Rcos(\Phi)tan(\Theta) \quad (7)$$

$$\dot{\Theta} = Qcos(\Phi) + Rsin(\Phi) \quad (8)$$

$$\dot{\Psi} = (Qsin(\Phi) + Rcos(\Phi))sec(\Theta) \quad (9)$$

$$\begin{bmatrix} \dot{P}_N \\ \dot{P}_E \\ \dot{P}_D \end{bmatrix} = \begin{bmatrix} c_\theta c_\psi & s_\phi s_\theta c_\psi - c_\phi s_\psi & c_\phi s_\theta c_\psi + s_\phi s_\psi \\ c_\theta s_\psi & s_\phi s_\theta s_\psi + c_\phi c_\psi & c_\phi s_\theta c_\psi - s_\phi c_\psi \\ -s_\theta & s_\phi c_\theta & c_\phi c_\theta \end{bmatrix} \begin{bmatrix} u \\ v \\ w \end{bmatrix} \quad (10)$$

These equations combined with the non-dimensional stability and control derivatives provided by Roskam [6], which are used to determine the forces and moments. An example of the equation used to find the moment about the y-axis is shown in Equation 11.

$$M = \bar{q}S\bar{c}(C_{m_0} + C_{m_\alpha}\alpha + C_{m_{\delta h}}\delta_h + C_{m_q}\frac{\bar{c}q}{2V_B}) \quad (11)$$

The nonlinear equations of motion were integrated using the Euler integration method, the basic theory of which is presented in Equation 12.

$$x(n) = f(x(n-1)) * \Delta t + x(n-1) \quad (12)$$

This integration was performed using a MATLAB program. It was also necessary to determine a trim condition for the aircraft. This was achieved by utilizing the MATLAB Symbolic Toolbox. The trim condition was to find the condition when all the forces and moments are zero. it is assumed that only u, v,  $\Theta$ , and Thrust are changing for the trim condition. The trim conditions found are given in Table 1.

	Trim Conditions
$V_B$	875.8 ft/s
$\Theta_1$	2.47 deg
Altitude	35000 ft
Weight	39000 lb
Thrust	2986 lb
Horizontal Stabilizer Incidence	0.7678 deg

**Table 1 The Trim Conditions of the F-4 Linear Model**

After trimming the aircraft, the model was then verified using a doublet in all the control surfaces and compared to the linear models for the F-4.

## B. Non-linear to linear Derivation

While the nonlinear model for an aircraft provides a good representation of the aircraft's motion, the nonlinear equations do not yield an easily quantifiable response to control inputs. However, linear models have responses that can be easily predicted. The process for transitioning from the nonlinear equations of motion to a linear state-space model is outlined in Appendix A; a brief explanation is provided here.

The derivation of the linear state-space model for the F-4 begins with the non-linear equations of motion, displayed by Equations 1 - 9 above. These equations are then linearized using the small perturbation assumptions described by Roskam [6]. The perturbed equations are then simplified by assuming straight, level, steady-state flight. The perturbed force and moment are then determined using the quasi-steady model for perturbed forces and moments, as explained by Roskam [6]. The perturbed forces and moments are then put into the perturbed equations of motion. These equations are then arranged into the longitudinal and lateral state-space models. The state-space models used for the Learjet-25 are similar to the models used for the F-4 but they include some different assumptions. The changes include assuming that  $W_1$  is not zero and having a different equation for  $\phi$  but the overall process is the same.

## C. Linear system theory

### 1. F-4 Linear Model

The linear models of the F-4 Phantom were created to analyze the overall behavior of the F-4 in both the longitudinal and lateral directions. These linear models are much simpler to understand than nonlinear models, and their simplified answers make predicting aircraft responses easier. One of the downsides of linear state-space models is that they can only be perturbed about a trim point not the entire flight envelope. The trim condition used for the F-4 model is shown in Table 2.

	F-4 linear model trim conditions
$U_1$	876.1 ft/s
$\Theta_1$	2.6 deg
Altitude	35000 ft
Weight	39000 lb

Table 2 The Trim Conditions of the F-4 Linear Model

By making Equations 1-9 linear and combining them into a state-space model, the aircraft's stability and other system characteristic as well as control system design can be determined. The longitudinal and lateral state-space models for the F-4 are shown as Equation 13 and Equation 14 respectively. Both equations and the values of the coefficients for the F-4 are given by Roskam [6].

$$\begin{bmatrix} 1 & 0 & 0 & 0 \\ 0 & (U_1 - Z_{\dot{\alpha}}) & 0 & 0 \\ 0 & -M_{\dot{\alpha}} & 1 & 0 \\ 0 & 0 & 0 & 1 \end{bmatrix} \begin{bmatrix} \dot{u} \\ \dot{\alpha} \\ \dot{q} \\ \dot{\theta} \end{bmatrix}_{long} = \begin{bmatrix} X_u & X_\alpha & X_q & -g \cos(\Theta_1) \\ Z_u & Z_\alpha & (U_1 + Z_q) & -g \sin(\Theta_1) \\ M_u & M_\alpha & M_q & 0 \\ 0 & 0 & 1 & 0 \end{bmatrix} \begin{bmatrix} u \\ \alpha \\ q \\ \theta \end{bmatrix} + \begin{bmatrix} X_{\delta e} \\ Z_{\delta e} \\ M_{\delta e} \\ 0 \end{bmatrix} \delta e \quad (13)$$

$$\begin{bmatrix} 1 & 0 & 0 & -\frac{I_{xz}}{I_{xx}} \\ 0 & 1 & 0 & 0 \\ 0 & 0 & U_1 & 0 \\ -\frac{I_{xz}}{I_{zz}} & 0 & 0 & 1 \end{bmatrix} \begin{bmatrix} \dot{p} \\ \dot{\phi} \\ \dot{\beta} \\ \dot{r} \end{bmatrix}_{lat} = \begin{bmatrix} L_p & 0 & L_\beta & L_r \\ 1 & 0 & 0 & 0 \\ Y_p & g \cos(\Theta_1) & Y_\beta & Y_r - U_1 \\ N_p & 0 & N_\beta & N_r \end{bmatrix} \begin{bmatrix} p \\ \phi \\ \beta \\ r \end{bmatrix} + \begin{bmatrix} L_{\delta a} & L_{\delta r} \\ 0 & 0 \\ Y_{\delta a} & Y_{\delta r} \\ N_{\delta a} & N_{\delta r} \end{bmatrix} \begin{bmatrix} \delta a \\ \delta r \end{bmatrix} \quad (14)$$

These equations cannot be used in their current form. To be used they must be in the form shown in Figure 15.

$$\dot{x} = \mathbf{A}\vec{x} + \mathbf{B}\vec{u} \quad (15)$$

To get them into the correct form the following conversion must be done.

$$C' \dot{x} = A' \vec{x} + B' \vec{u} \rightarrow \dot{x} = C'^{-1} A' \vec{x} + C'^{-1} B' \vec{u} \rightarrow \dot{x} = \mathbf{A}\vec{x} + \mathbf{B}\vec{u} \quad (16)$$

The corrected state-space models were determined in and used to find the transfer functions, eigenvalues, and bode plots of the aircraft through MATLAB functions. The functions used to analyses linear systems were damp, lsim, bode and ss2tf. These were used for all linear modes. The behavior of the aircraft was analyzed by applying a doublet to the models. There will be a doublet for each of the three inputs which are the elevator, ailerons and rudder. The input for this system is in radians. The responses to these doublets are analyzed later in this paper.

## 2. Learjet-25 Linear Model

The Learjet-25 longitudinal SS model was created using an approach similar to the F-4. However, the matrices used by Dr. Tom Berger's analysis were slightly different than those presented by Dr. Roskam. Dr. Berger's state-space matrices do not assume a zero velocity in the z direction and have a different equation for  $\phi$ . The flight stability and control derivatives, the trim state, and the matrix structure were taken from Berger [8]. Dr. Berger's paper actually presents dimensional stability and control derivatives for two different configurations. Both configurations were analyzed in this report. The derivatives of the two configurations varied slightly. This will likely lead the doublet responses for the two configurations being similar to each other. The trim conditions for both configurations are shown in Table 3.

	Configuration 1	Configuration 2
$U_1$	422.0 ft/s	422.0 ft/s
$\Theta_1$	2.378 deg	2.882 deg
Altitude	15000 ft	15000 ft
Thrust( $\delta_{T_0}$ )	1366.3 lb	1455.9 lb
Elevator Deflection( $\delta_{e_0}$ )	-4.128 deg	-3.968 deg

Table 3 The Trim Conditions of the Learjet Linear Model

The structure of the matrix used to create the longitudinal and lateral state-space model can be seen in Equation 17 and 18. It can be seen that these models use  $w$  and  $v$  instead of  $\alpha$  and  $\beta$  along with the different assumptions discussed above. There is also an additional control input that was not on the F-4 linear model: Thrust.

$$\begin{bmatrix} \dot{u} \\ \dot{w} \\ \dot{q} \\ \dot{\theta} \end{bmatrix} = \begin{bmatrix} X_u & X_w & X_q - W_1 & -g \cos \Theta_1 \\ Z_u & Z_w & Z_q - U_1 & -g \sin \Theta_1 \\ M_u & M_w & M_q & 0 \\ 0 & 0 & 1 & 0 \end{bmatrix} \begin{bmatrix} u \\ w \\ q \\ \theta \end{bmatrix} + \begin{bmatrix} X_{\delta_e} & X_{\delta_T} \\ Z_{\delta_e} & Z_{\delta_T} \\ M_{\delta_e} & M_{\delta_T} \\ 0 & 0 \end{bmatrix} \begin{bmatrix} \delta_e \\ \delta_T \end{bmatrix} \quad (17)$$

$$\begin{bmatrix} \dot{v} \\ \dot{p} \\ \dot{r} \\ \dot{\phi} \end{bmatrix} = \begin{bmatrix} Y_v & Y_p + W_1 & Y_r - U_1 & g \cos \Theta_1 \\ L_v & L_p & L_r & 0 \\ N_v & N_p & N_r & 0 \\ 0 & 1 & \tan \Theta_1 & 0 \end{bmatrix} \begin{bmatrix} v \\ p \\ r \\ \phi \end{bmatrix} + \begin{bmatrix} Y_{\delta_a} & Y_{\delta_r} \\ L_{\delta_a} & L_{\delta_r} \\ N_{\delta_a} & N_{\delta_r} \\ 0 & 0 \end{bmatrix} \begin{bmatrix} \delta_a \\ \delta_r \end{bmatrix} \quad (18)$$

Like the F-4 linear model, the Learjet linear models will be analyzed using MATLAB functions to get the eigenvalues, transfer function, and Bode plots. Doublet responses will be used in validation. The systems response to the four control doublets will be presented. The control inputs are thrust, elevator, aileron and rudder. The inputs for the control surfaces are in degrees and the input for thrust is in pounds. select results from these analyses will be discussed in the validation section.

## D. Controller Theory

**Negative Feedback Loops** Many control systems utilize negative feedback loops to regulate system behavior. In a typical feedback configuration, the output of the system (also called the plant) is measured and compared against a desired reference input. The difference between the reference input and the measured output, known as the error signal, is then used by the controller to compute a corrective control input. This corrective action drives the system toward the

desired state by minimizing the error over time. Negative feedback inherently stabilizes the system, improves disturbance rejection, and reduces sensitivity to parameter variations, making it a foundational principle in control system design.

**PID Controllers** Proportional-integral-derivative (PID) controllers are widely used in flight control systems due to their simplicity and effectiveness in stabilizing dynamic systems. A PID controller can be added to a feedback loop to modulate the system's error input  $e(t)$ . The controller adjusts the input using three terms: the present error, the accumulation of errors, and the rate of change in the current error. The control equation for a PID controller can be expressed as:

$$u(t) = K_p e(t) + K_i \int e(t) dt + K_d \frac{d}{dt} e(t) \quad (19)$$

Where:

- $u(t)$  is the control input,
- $e(t)$  is the error signal (e.g., the difference between the desired and measured pitch angle),
- $K_p$  is the proportional gain,
- $K_i$  is the integral gain,
- $K_d$  is the derivative gain.

The proportional term ( $K_p e(t)$ ) provides an immediate response to the current error, the integral term ( $K_i \int e(t) dt$ ) eliminates the steady-state error by integrating the error over time, and the derivative term ( $K_d \frac{d}{dt} e(t)$ ) uses the rate of change of the error to add damping to the response.

By applying the Laplace transform to the time-domain representation of the PID controller, the corresponding transfer function in the s-domain is obtained. This transfer function expresses the controller's behavior in terms of proportional, integral, and derivative components as follows:

$$G_c(s) = K_p + \frac{K_i}{s} + K_d s \quad (20)$$

The transfer function shows that the PID controller introduces a pole at the origin (due to the integral term) and zeros associated with the proportional and derivative actions, thereby shaping the system dynamics to achieve desired performance characteristics such as stability, steady-state accuracy, and transient response improvements.

**PID Implementation in Roll/Pitch-Hold Controllers** The pitch-hold controller uses a negative feedback loop with a standard PID configuration. Because the derivative term is highly sensitive to high-frequency signals, present in noisy sensors or sensitive systems, the derivative action can excessively amplify the noise, leading to large, rapid fluctuations in the control input, which may destabilize the system.

To mitigate this, a lowpass filter is added to the derivative term. In the Laplace domain, the filtered response now becomes:

$$G_c(s) = K_p + \frac{K_i}{s} + \frac{K_d s}{\tau s + 1} \quad (21)$$

With  $\tau$  being the time constant for the lowpass filter. A larger  $\tau$  value produces slower responses to the derivative responses. This prioritizes noise suppression at the expense of response time.

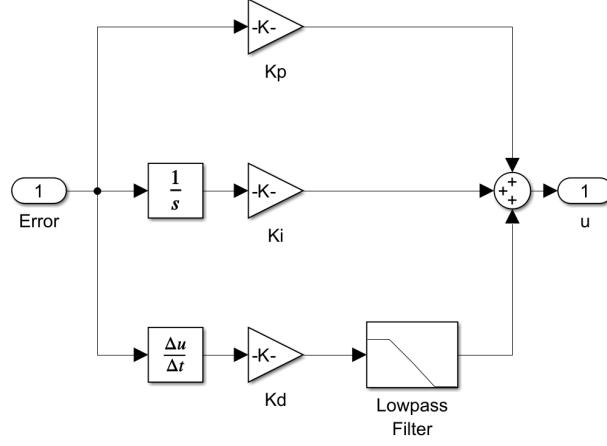


**Fig. 2 PID controller**

The PID controller can be added to a negative feedback loop, as shown in Figure 3. This controller features a 0.005 second delay to account for any resistances and computational delays. The control surface actuator is modeled using a rate limiter with a saturation block to keep the angle between  $\pm 15^\circ$ . The loop is designed around a transfer function to model system behavior.

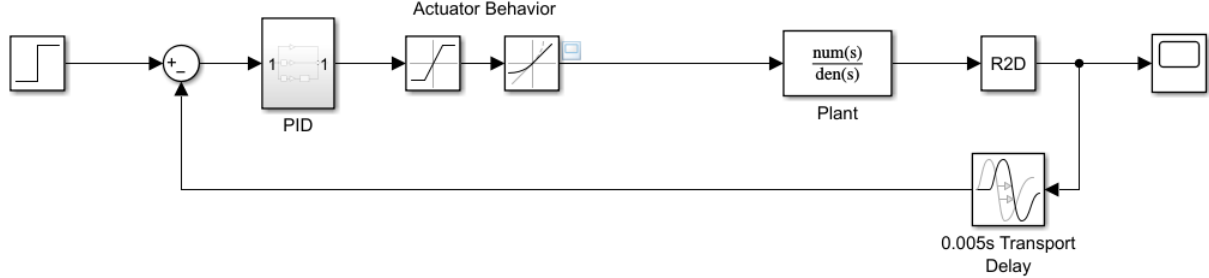


**Fig. 3 Example Feedback Loop Controller Design**

**Feedback Loop Transfer Function** Identifying each component of the control architecture allows the overall system transfer function,  $\frac{\Theta(s)}{\Theta_c(s)}$ , to be systematically derived.

The elements of the system are defined as follows:

- **PID Controller:**

$$G_c(s) = K_p + \frac{K_i}{s} + \frac{K_d s}{\tau s + 1}$$

Where  $\tau$  represents the time constant of the low-pass filter applied to the derivative term to suppress high-frequency noise.

- **Aircraft Plant:**

$$G_p(s) = \frac{\text{num}(s)}{\text{den}(s)}$$

Where  $\text{num}(s)$  and  $\text{den}(s)$  represent the numerator and denominator polynomials characterizing the aircraft's dynamic response.

The error signal at the summing junction of the feedback loop is defined as:

$$E(s) = \Theta_c(s) - \Theta(s) \quad (22)$$

Substituting the system dynamics into this relationship yields:

$$E(s) = \frac{\Theta_c(s)}{1 + G_c(s)G_p(s)} \quad (23)$$

From this, the closed-loop transfer function of the system (command input to measured output) is derived as:

$$\boxed{\frac{\Theta(s)}{\Theta_c(s)} = \frac{G_c(s)G_p(s)}{1 + G_c(s)G_p(s)}} \quad (24)$$

Physical phenomena such as sensor and computation delays must also be considered to model the system behavior more realistically. Measurements of state variables are subject to time delays due to signal transmission, processing time, and actuator response lag. This transport delay is incorporated into the feedback loop.

In the time domain, a transport delay of  $T_d$  seconds is represented as:

$$x_{\text{delayed}}(t) = x(t - T_d)$$

and in the Laplace domain by the exponential factor:

$$X_{\text{delayed}}(s) = e^{-T_d s} X(s)$$

Since the delay affects only the measurement and not the forward control path, it appears exclusively in the denominator of the closed-loop transfer function. Incorporating the transport delay modifies the system transfer function to:

$$\boxed{\frac{\Theta(s)}{\Theta_c(s)} = \frac{G_c(s)G_p(s)}{1 + G_c(s)G_p(s)e^{-T_d s}}} \quad (25)$$

**PID Tuning** Finding the gain parameter values for the PID controller is the next problem to solve. When tuning the controller, several factors should be considered.

- **Rise Time:** How fast the system responds to a command.
- **Overshoot:** How much the system exceed the desired response.
- **Settling Time:** How long it takes the system to settle within a certain percentage of the final value.
- **Steady-State Error:** the final difference between commanded and actual output.
- **Disturbance Rejection:** How well the system can reject wind gusts, turbulence, sensor noise, etc...

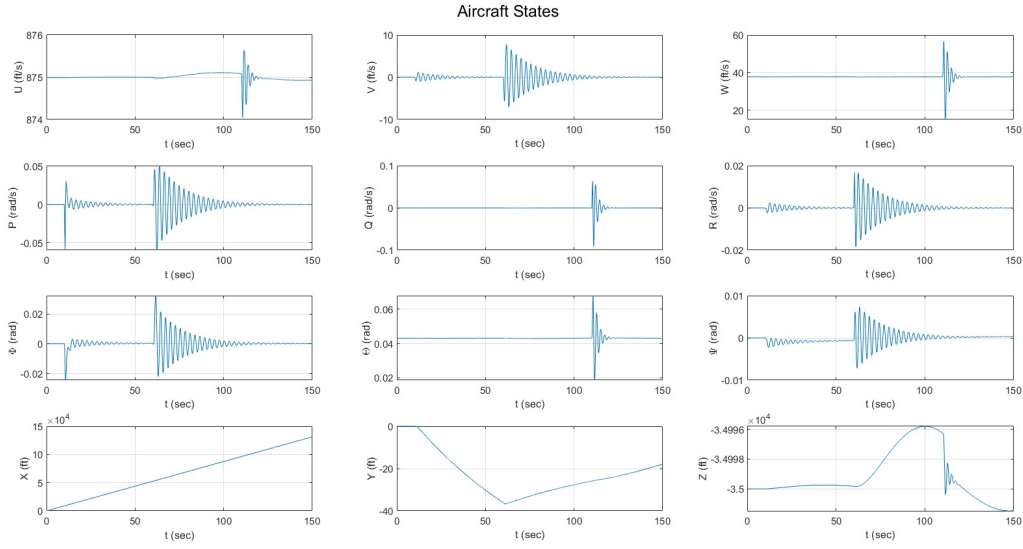
The proportional, integral, and derivative gains ( $K_p$ ,  $K_i$ , and  $K_d$ ) each affect system response differently. Increasing  $K_p$  reduces rise time but can cause overshoot or instability if too high.  $K_i$  eliminates steady-state error but may introduce oscillations and slow settling.  $K_d$  adds damping and improves transient response, though excessive values can amplify noise and lead to erratic control.

## IV. Model Validation

### A. Doublet Responses

#### 1. F-4 Non-Linear Doublet Responses

The non-linear system of the F-4 has the same inputs as the linear system, but different implementation. Instead of the input being multiplied by the **B** matrix and then added to the **A** matrix in the state-space model, the non-linear model applies its inputs directly to the forces and moments of the aircraft. Figure 4 shows the effect of aileron, rudder, and elevator doublets on the F-4 nonlinear system. The doublets are a half-second down, half-second up with a one degree deflection magnitude.



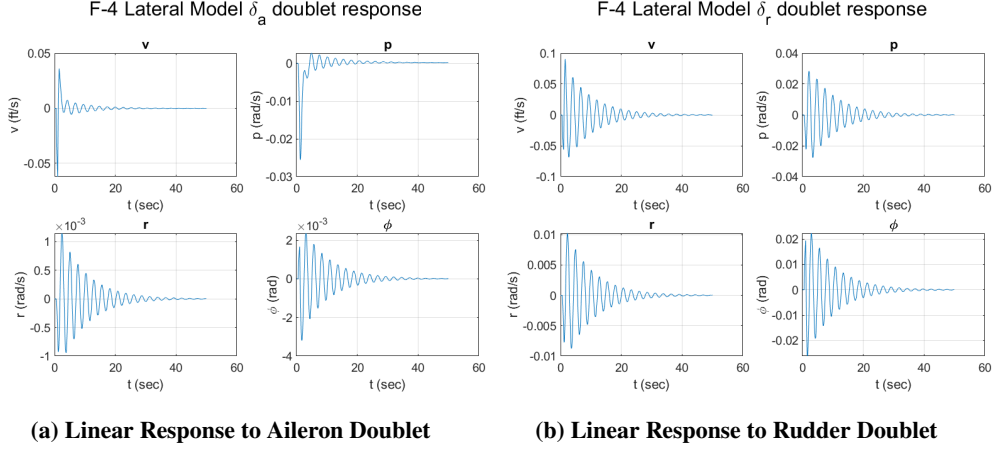
**Fig. 4 Nonlinear responses to aileron, rudder, and elevator doublets at 10, 60, and 110 seconds, respectively**

Figure 4 shows the longitudinal and lateral states mostly do not affect each other; however, relationships between the two can be observed in two specific instances. First, the  $U$  component of velocity slightly increases in response to the rudder doublet. This is caused by the  $PV$  term in Equation 1, which is the velocity in the  $x$ -direction equation. Second, the  $Z$  position changes due to aileron and rudder doublet input. This is due to a combination of velocity in the  $y$ -direction and rotation about the  $x$ -axis, which caused a decrease in the altitude for both the aileron and rudder doublet.

It can also be seen the rudder has a greater effect on the lateral states than the aileron. The lateral states all exhibit some evidence of a Dutch roll mode after both the aileron and rudder doublets. The roll mode can also be seen in  $P$  and  $\Phi$  as a result of the aileron doublet. The short-period mode is evident in the longitudinal states, and the Phugoid mode is visible in the last 30 seconds of  $U$ , where a small oscillation is observed. This shows that the nonlinear system can demonstrate the longitudinal and lateral modes of the aircraft, even if the modes cannot be quantified as they are in a linear model. These results will be compared to the results from the linear F-4 model in a section.

## 2. Linear F-4 Model

For the linear model of the F-4, values of dimensional stability and control derivatives were taken from Roskam [6], as stated above. The F-4 was subjected to a half second down, half second up, one degree doublet for the aileron, elevator, and rudder control surfaces. Figures 5 and 6 show the stability characteristics of the aircraft. The Phantom is completely laterally stable, but is unstable in the longitudinal direction. This is most apparent in  $u$ , but does show up in all of the longitudinal states. This is due to an instability in an unusual, positive value for one of the roots. The F-4 linear model has two complex and two real eigenvalues which is not normal for a longitudinal system. This is most likely caused by the assumptions made when deriving the state-space model because the nonlinear model does not show such instability.



**Fig. 5 F-4 Linear Lateral Doublet Responses**

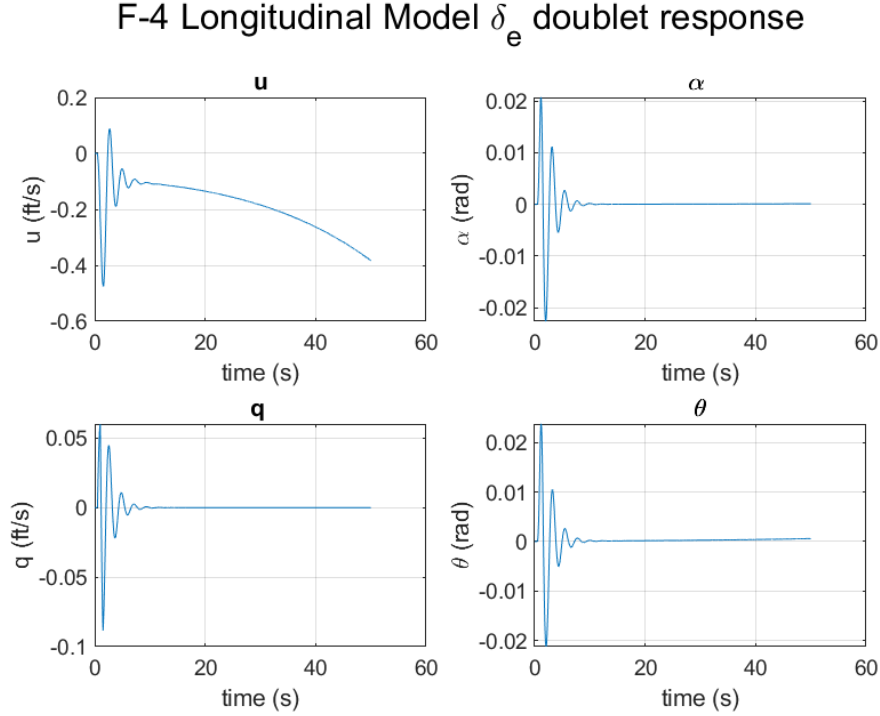


**Fig. 6 Linear Response to Elevator Doublet**

### 3. Linear Learjet Model

To linearly model the Learjet, two configurations were taken from Berger [8]. These configurations will be analyzed separately, as their stability results differ. To analyze each of these configurations, they were broken into their Lateral and Longitudinal components, and then subjected to a half second down, half second up, one degree doublet for the aileron, elevator, and rudder control surfaces and a 100 lbf doublet for the thrust.

For Configuration 1, Figure 7 displays the lateral system response to induced doublet aileron and rudder inputs. These figures show a stable system under trim, with all control aspects stabilizing quickly to set values. Continuing Configuration 1, Figure 8 shows the longitudinal system response to induced doublets. For these responses,  $\alpha$  and  $q$  stabilize quickly, while  $u$  and  $\theta$  take much longer to come to a steady state.

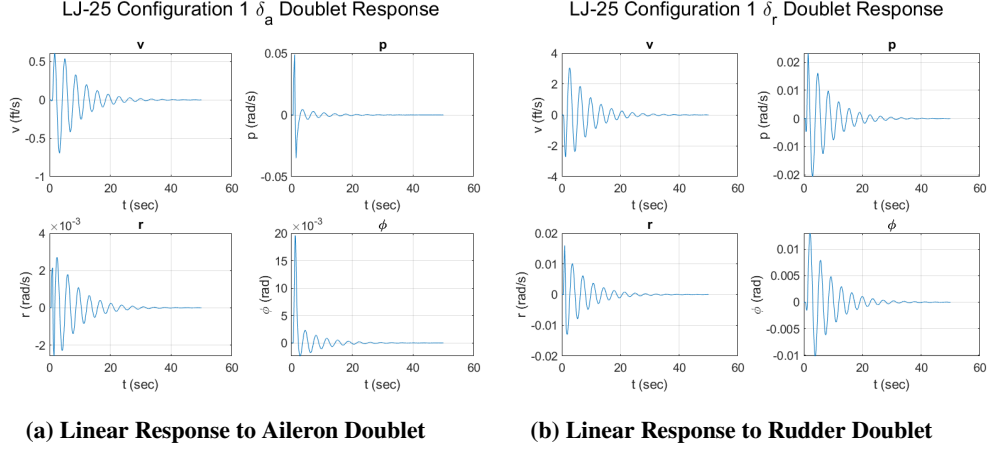


**Fig. 7 Linear Lateral Doublet Responses - Configuration 1**

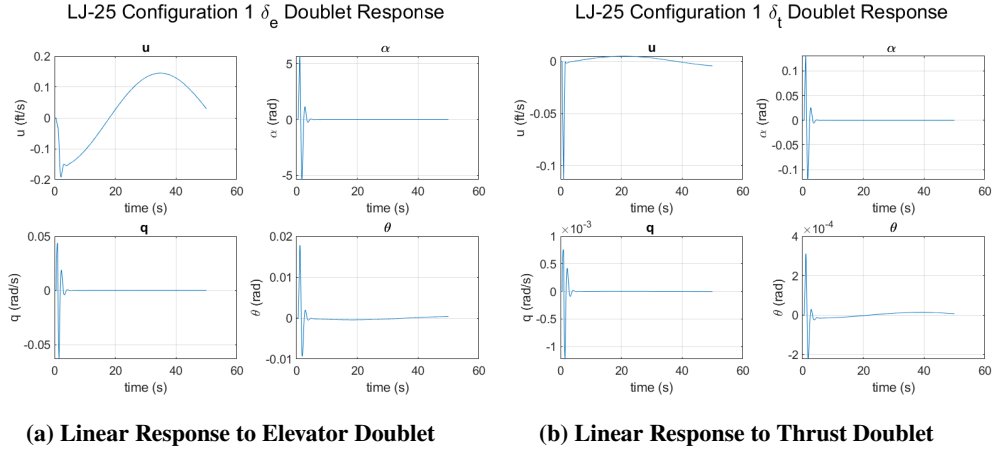


**Fig. 8 Linear Longitudinal Doublet Responses - Configuration 1**

For Configuration 2, Figure 9 shows that lateral system the system response to induced doublets. These figures showcase an unstable system, with  $r$  and  $\phi$  remaining marginally unstable.  $v$  and  $p$  are stable however, and converge to a steady state. The longitudinal system response can be observed in Figure 10.  $\alpha$  and  $q$  stabilize rapidly, while  $u$  and  $\theta$  take much longer to reach a steady state.

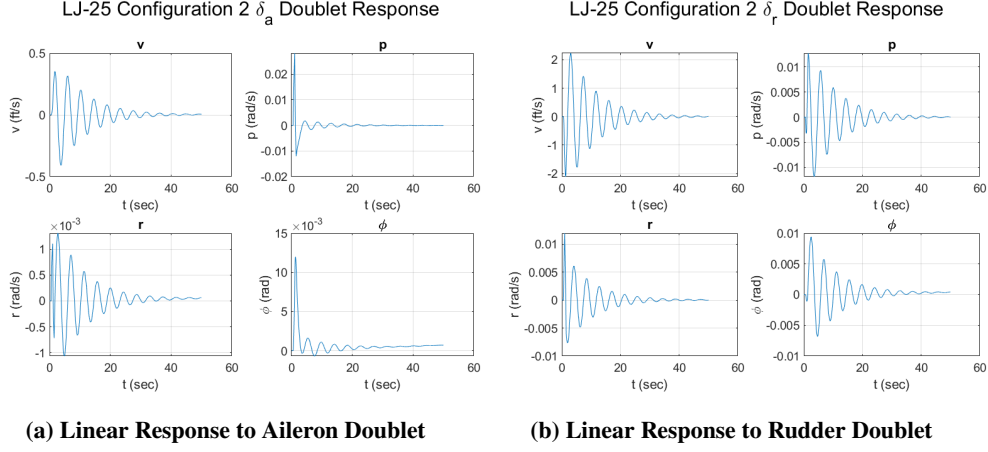


**Fig. 9 Linear Lateral Doublet Responses - Configuration 2**

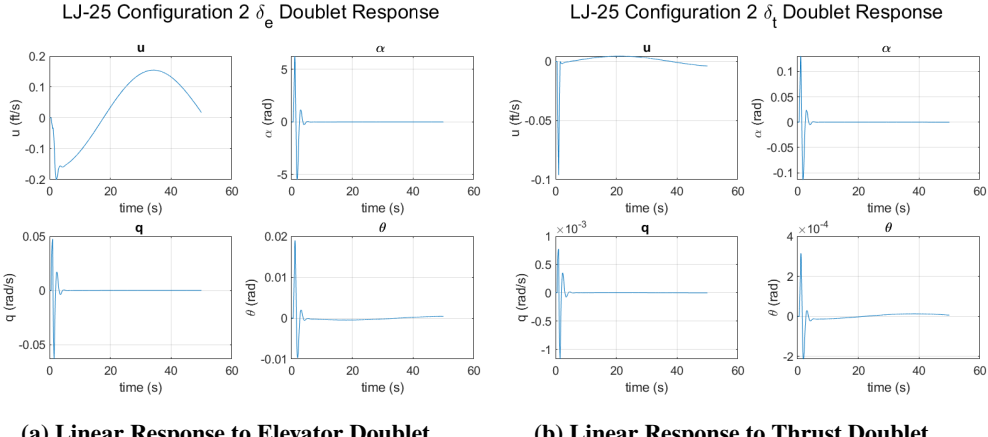


**Fig. 10 Linear Longitudinal Doublet Responses - Configuration 2**

These figures can also be used to identify the various different aircraft modes. In the longitudinal figures, the Phugoid mode influences long-period convergence times in the  $u$  and  $\theta$  responses. The short-period mode is also displayed in the quick convergence times seen in the  $q$  and  $\alpha$  reactions.

In the lateral figures, the roll and spiral modes are seen in the graphs of  $p$  and  $\phi$ . The spiral mode's instability is also found here, with configuration 2 being unstable and most noticeable in  $\phi$ . The Dutch roll mode is visible in the reactions of  $r$  and  $v$ . The Dutch roll mode is stable, and this is again found in configuration 2. The  $v$  doublet response appears stable, but its  $r$  response is unstable due to the unstable spiral mode.

## B. Comparisons

### 1. F-4 Linear vs Nonlinear

Comparing the linear and nonlinear F-4 model's doublet response results in several differences between them. The  $U$  response of the nonlinear state is stable in its doublet response, while the linear state is unstable. This is likely because of poor assumptions found in the Roskam textbook. However, on other nonlinear state responses, the doublet responses match with the expected aileron and rudder reactions at their specific time frame. However, there are differences in the magnitude for some states based on the interaction between lateral and longitudinal directions in the nonlinear response.

## 2. Learjet Configuration 1 vs Configuration 2

The differences between the Learjet configurations are shown mainly in the lateral doublet response. In Configuration 1, the lateral response is stable across all states, but in Configuration 2, the  $\phi$  and  $r$  states are unstable. This is reflected in the eigenvalues of the systems. The longitudinal response for Configuration 1 and 2 are very similar, achieving the same shapes and steady state values for both configurations.

## C. Transfer functions

The linear F-4 model along with the linear models for Configurations 1 and 2 of the Learjet 25 all initially produced non-decomposed fourth-order transfer functions. In their non-decomposed states, these transfer functions are difficult to interpret. However, by using the residue function in MATLAB the functions can be decomposed, typically into two second-order systems, which are much easier to analyze. When used in conjunction with the damp function in MATLAB, all the characteristics of the system can be extracted. This information can be used to do system identification and predict the model's behavior.

The data extracted from the transfer functions includes decomposed transfer functions, eigenvalues, poles, natural frequencies, damping ratios, and time constants. With these values, it is easy to validate the behavior in various graphical representations of the aircraft's state-space models. Below, a few of the transfer functions from the analysis are highlighted.

The first two transfer functions below can be compared to observe the impact of two inputs, elevator deflection and thrust change, on the state of pitching rate,  $q$ . These transfer functions are derived from the linear state-space model of configuration 1 of the Learjet 25. Although the impact of both of these inputs on the pitch rate is small, which can be observed by looking at the zero polynomial in the numerator which governs the amplitude of the output. Also, though they are both small for lower frequencies (which is really the only predictable input frequency range for these models) it is plain to see that the magnitude of the pitch rate response to the elevator input is many orders of magnitude higher than the thrust response.

$$\frac{q}{\delta_e} = \left( \frac{-0.1918 s - 0.246}{s^2 + 3.086 s + 12.3} \right) \left( \frac{-0.0001171 s + 0.0001679}{s^2 + 0.006208 s + 0.008397} \right)$$

$$\frac{q}{\delta_T} = \left( \frac{-3.884 \times 10^{-5} s - 3.102 \times 10^{-5}}{s^2 + 3.086 s + 12.3} \right) \left( \frac{5.789 \times 10^{-7} s + 2.118 \times 10^{-8}}{s^2 + 0.006208 s + 0.008397} \right)$$

The next transfer function represents the F-4's pitch rate to the elevator deflection input transfer function. As expected, the F-4's pitch rate response to elevator deflection is much more dramatic and responsive than the Learjet. The Learjet as a business jet is not meant to be as acrobatic as a fighter plane such as the F-4 which needs to be able to do quick maneuvers. Another observation about all of these transfer functions is that the short period mode (in the first parentheses of each transfer function) has a greater amplitude than the long-period mode, which is normal and desirable in most applications.

$$\frac{q}{\delta_e} = \left( \frac{-11.37 s - 5.744}{s^2 + 1.258 s + 8.106} \right) \left( \frac{-0.01089 s - 0.001086}{s^2 - 0.001006 s - 0.001533} \right)$$

The following transfer functions highlight the relationships between roll rate,  $p$  and aileron or rudder deflection angle inputs. These transfer functions are not as easily evaluated upon first inspection. But by extracting the eigenvalues from both parts of the transfer function, it is easier to tell which mode each part represents. One part will represent Dutch roll modes for which there will be a pair of complex eigenvalues. The part representing the roll and spiral modes will produce two real eigenvalues. Beginning with the transfer functions for Configuration 2 of the Learjet below, the difference in the responses are more apparent in the denominator, which is reflected in the eigenvalues.

$$\frac{p}{\delta_r} = \left( \frac{0.0281 s - 0.04618}{s^2 + 0.2108 s + 2.124} \right) \left( \frac{-0.0108 s - 0.0003686}{s^2 + 1.156 s - 0.02318} \right)$$

Eigenvalues:

$$\underbrace{-0.1054 \pm 1.4471j}_{\begin{array}{l} \text{Dutch roll mode} \\ \text{Roll mode} \end{array}} \quad \xleftarrow{\text{from first denominator}}$$

$$\underbrace{-1.1375, -0.0185}_{\begin{array}{l} \text{Spiral mode} \end{array}} \quad \xleftarrow{\text{from second denominator}}$$

$$\frac{p}{\delta_a} = \left( \frac{-0.008231 s - 0.003696}{s^2 + 0.2108 s + 2.124} \right) \left( \frac{-0.06362 s + 0.0002069}{s^2 + 1.156 s - 0.02318} \right)$$

Eigenvalues:

$$\underbrace{-0.1054 \pm 1.4471j}_{\begin{array}{c} \text{Dutch roll mode} \\ \text{Roll mode} \end{array}} \quad \xleftarrow{\text{from first denominator}}$$

$$\underbrace{-1.1375, \quad -0.0185}_{\begin{array}{c} \text{Spiral mode} \\ \text{Spiral mode} \end{array}} \quad \xleftarrow{\text{from second denominator}}$$

As expected, the eigenvalues are the same for these two responses. The only difference resides in the numerator which shows that the aircraft has a greater response to rudder deflection than it does to aileron deflection. The next two transfer functions show the relationship between roll rate and rudder/aileron deflection for the F-4.

$$\frac{p}{\delta_r} = \left( \frac{7.218 s - 9.249}{s^2 + 0.2297 s + 5.74} \right) \left( \frac{-5.492 s + 0.02827}{s^2 + 1.351 s + 0.01755} \right)$$

$$\frac{p}{\delta_a} = \left( \frac{1.026 s - 0.01685}{s^2 + 0.2297 s + 5.74} \right) \left( \frac{8.747 s + 5.15 \times 10^{-5}}{s^2 + 1.351 s + 0.01755} \right)$$

Eigenvalues:

$$\underbrace{-0.1149 \pm 2.3909j}_{\begin{array}{c} \text{Dutch roll mode} \\ \text{Roll mode} \end{array}} \quad \xleftarrow{\text{from first denominator}}$$

$$\underbrace{-1.3372, \quad -0.0130}_{\begin{array}{c} \text{Spiral mode} \\ \text{Spiral mode} \end{array}} \quad \xleftarrow{\text{from second denominator}}$$

Once again, the roll rate is much more pronounced in the F-4 fighter jet than it is in the Learjet 25 business jet (regardless of configuration). These transfer functions are used to create Bode plots to visualize frequency responses. The natural frequencies of which can be easily extracted from the complex part of the decomposed transfer function along with the damping ratios can be used to validate the Bode plots. These values are also helpful when evaluating the Bode plots, as they serve as "landmarks" or main characteristic points in the plots. The resonance peaks, for instance, occur at the natural frequencies of the Dutch roll, Phugoid, and short-period modes.

## D. Frequency Responses

The frequency response provides insight into how an aircraft's dynamic system reacts to sinusoidal inputs across a range of frequencies. It characterizes the stability and performance of the system in a given frequency domain, showing a picture of resonant behavior, phase lag, and gain variations. Through this frequency analysis, the Learjet-25 (Configuration 1) and the F-4 can be compared. Two notable frequency responses, and the focus of this section, are the roll and pitch rate responses. While other frequency response are still important, for brevity, only these two will be closely analyzed. All frequency responses can be found in Appendix D.

### 1. F-4 Frequency Response

Figure 11 shows the frequency response of the pitch rate in the F-4 model due to elevator command. Two notable items in this figure are the resonance bump and high phase angle. The resonance bump is indicative of the natural frequency of the aircraft, at which point the system responds most strongly to control commands. By decomposing transfer functions and looking at natural frequencies, this is the short period. At this bump, the magnitude nears 20 dB. This magnitude signifies the response of the aircraft in respect to input. At 0 dB, the response would be the same magnitude as the input. At 20 dB, the input is magnified by ten. A fighter jet like the F-4 is very responsive. So, a high magnitude at the natural frequency is appropriate. The phase angle of the F-4 is also very positive at the frequency

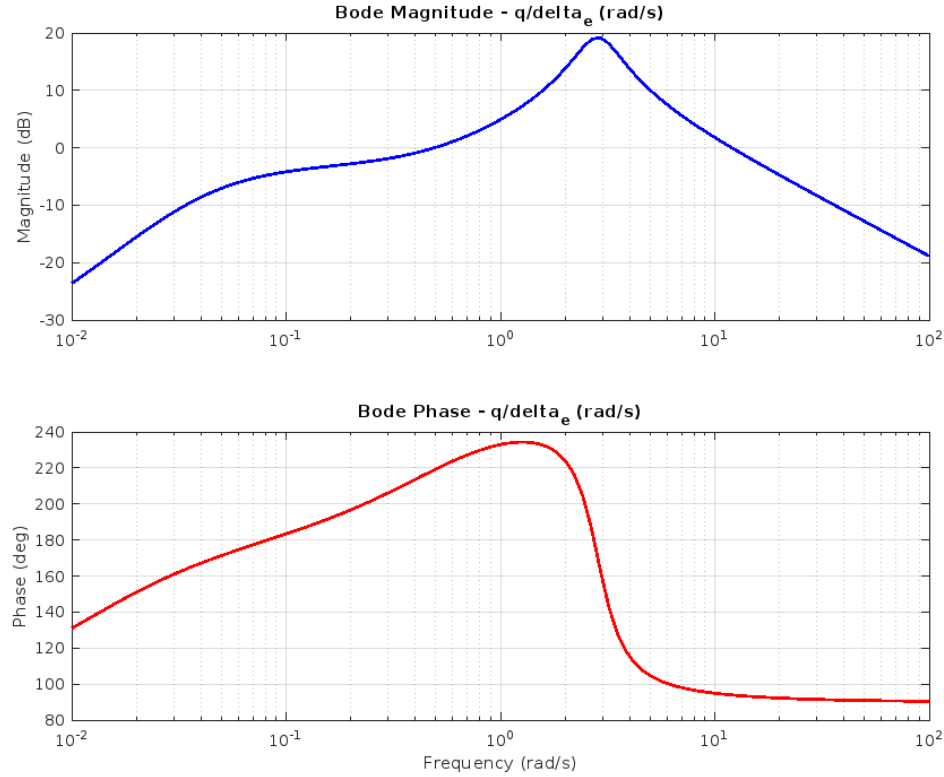


**Fig. 11 F-4 Bode Magnitude and Phase Plots of Pitch Rate Response to Elevator Command.**

ranges shown. The phase angle signifies the time shift between the input and output signals at a given frequency. A positive phase angle means the output leads the input. In this case, if an elevator input were applied, the pitch rate would reach its maximum before the elevator input does. For a highly responsive aircraft like the F-4, this high phase angle is fitting. It is worth noting that when analyzing phase angles they are measured in increments of 180 degrees and therefore, anything higher should not be directly recorded as the true phase angle.

The roll response of the F-4 due to aileron and rudder control input can be seen in Figure 12.

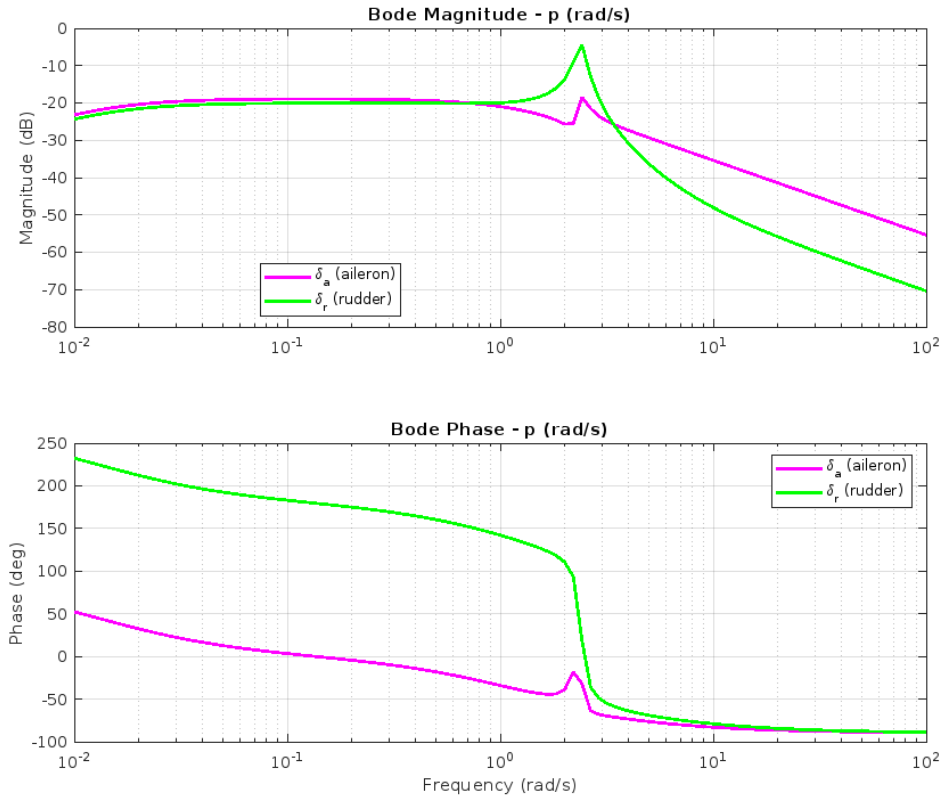


**Fig. 12 F-4 Bode Magnitude and Phase Plots of Roll Rate Response to Aileron and Rudder Command.**

Again, in this figure, the natural frequency can be seen at the bump in magnitude. The aileron and rudder input have the same natural frequency as they come from the same state space model. Both magnitudes remain negative, even at the natural frequency. This is to limit how responsive the F-4 is to roll input. If a roll maneuver is done too quickly, the aircraft could quickly become unstable or leave its flight envelope. A negative magnitude damps the input and prevents this. The phase angles of the aileron and rudder command are seen to have a large difference up until the natural frequency. The rudder output leads the input highly and drops at the natural frequency. The aileron output begins lagging the input after 0.1 rad/s. This signifies that higher frequency movements of the control stick will have a delayed response. Things like this are important for pilots to understand, and this is why frequency response is useful. Understanding that an aileron command will have a delayed response past a certain frequency can prevent over-correction.

## 2. Learjet-25 Frequency Response

The roll rate response from aileron and rudder command can be seen in Figure 13.

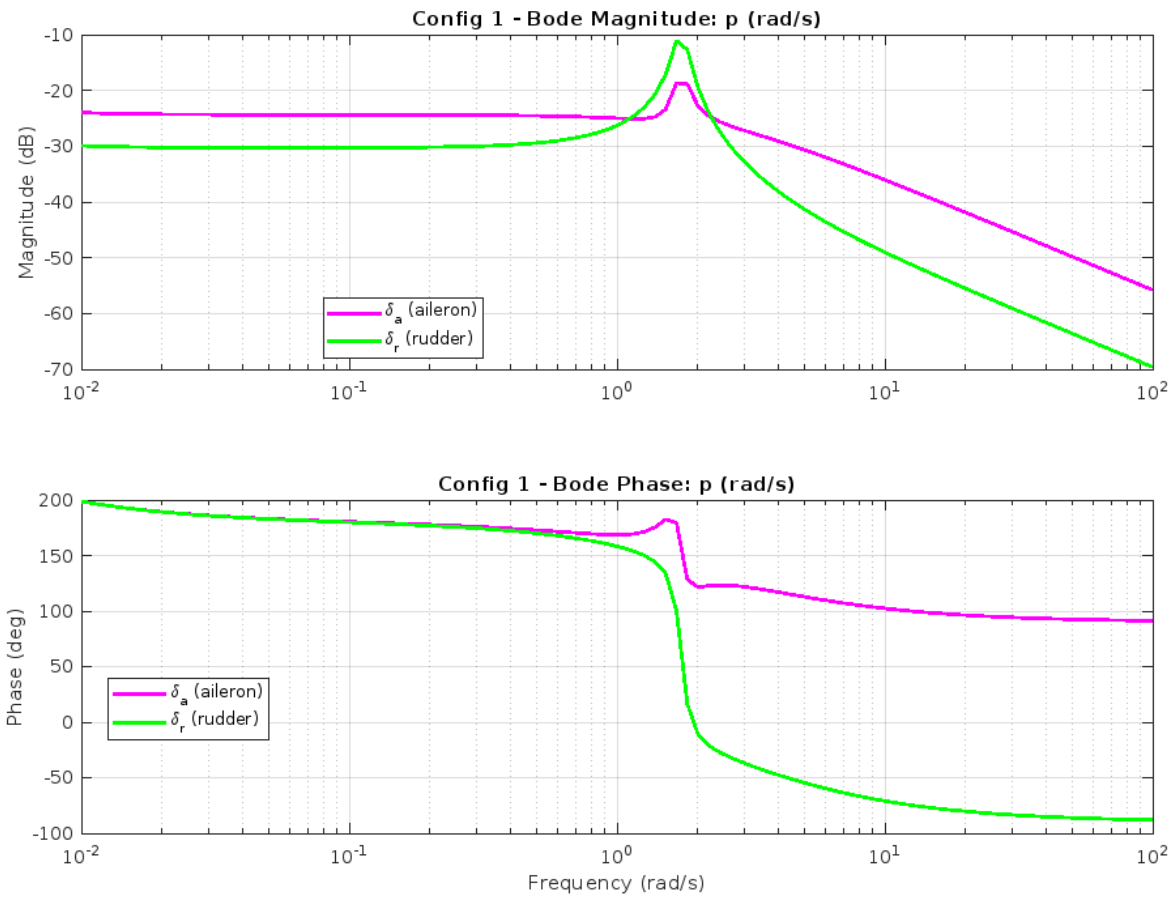


**Fig. 13 Learjet-25 Bode Magnitude and Phase Plots of Roll Rate Response to Elevator and Thrust Command.**

The natural frequency of these responses can be found from the resonance bump in Figure 13. At this frequency, the aileron and rudder have the most input magnitude, though the magnitude is negative. So, for roll rate, the Learjet is less responsive to both aileron and rudder input. The aircraft will not respond as greatly as the F-4. The aileron phase angle remains positive for the frequency ranges shown, with a drop after the natural frequency. The aileron command becomes less responsive past the natural frequency, but not as much as the rudder. The pitch rate response from the elevator and thrust command can be seen in Figure 14.

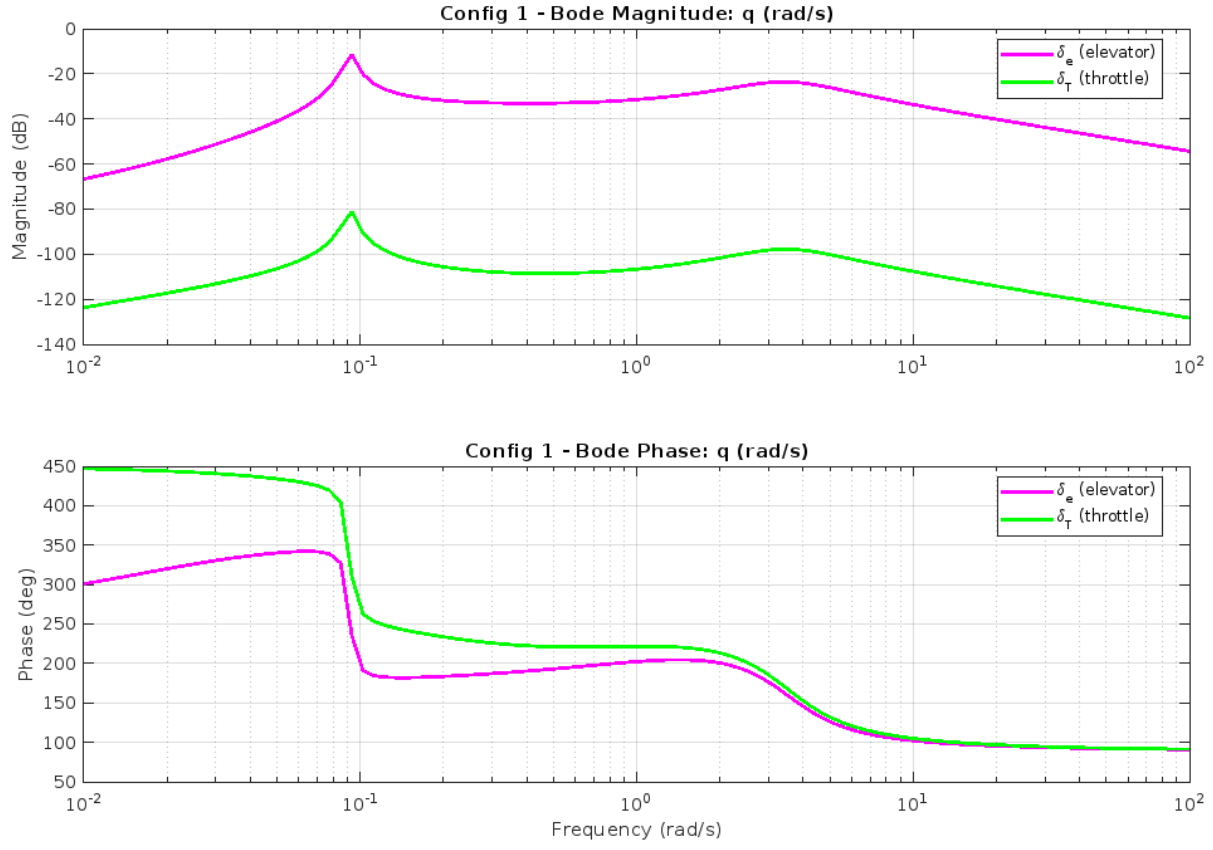


**Fig. 14 Learjet-25 Bode Magnitude and Phase Plots of Pitch Rate Response to Elevator and Thrust Command.**

The pitch rate response has a natural frequency but is not as significant as previous ones seen. The throttle magnitude is very negative, signifying it has little impact on the pitch rate of the aircraft. The elevator magnitude is higher, but still negative. The elevator command output is on the smaller side, which is appropriate for an aircraft like the Learjet. The Learjet's elevator is a much smaller portion of the aircraft when compared to the F-4. It would not be able to pitch nearly as quickly.

## V. Results

### A. Handling Qualities

Handling quality summarizes the ease with which the pilot can operate an aircraft and the precision with which the flight can be performed. The flight test data of high-performance aircraft can be analyzed using Neal-Smith, Bandwidth, and other handling quality criteria to provide information on the aircraft. The Military Specification 8785 criteria and the Cooper-Harper pilot rating scale were used for the two aircraft that were reviewed based on Roskam [6]. The first step to determine the handling qualities of the aircraft was to define their classes and flight phases. The Learjet-25 is defined as a business jet and falls under a Class 2 Airplane. The F-4 is a fighter-bomber plane and is a Class 4 airplane. Figure 15 shows how their classes were found using Roskam's table of similar aircraft and the MIL-F-8785C criteria, found in Roskam [6].

MIL-F-8785C	Examples	Civilian Equivalent	Examples
<b>Class I Small, light airplanes such as:</b> * Light utility * Primary trainer * Light observation	* Cessna T-41 * Beech T-34C * Rockwell OV-10A	Very Light Aircraft (VLA) and FAR 23 category airplanes	* Cessna 210 * Piper Tomahawk * Edgeley Optica
<b>Class II Medium weight, low-to-medium maneuverability airplanes such as:</b> * Heavy utility / search and rescue * Light or medium transport / cargo / tanker * Early warning / electronic counter-measures / airborne command, control or communications relay * Anti-submarine * Assault transport * Reconnaissance * Tactical Bomber * Heavy Attack * Trainer for Class II	* Fairchild C-26A/B * Fairchild C-123 * Grumman E-2C * Boeing E-3A * Lockheed S-3A * Lockheed C-130 * Fairchild OA-10 * Douglas B-60 * Grumman A-6 * Beech T-1A	FAR 25 category airplanes	* Boeing 737, * Airbus A 320 * McDowell MD-80
<b>Class III Large, heavy, low-to-medium maneuverability airplanes such as:</b> * Heavy transport / cargo / tanker * Heavy bomber * Patrol / early warning / electronic counter-measures / airborne command, control or communications relay * Trainer for Class III	* McDowell C-17 * Boeing B-52H * Lockheed P-3 * Boeing E-3D * Boeing TC-135	FAR 25 category airplanes	* Boeing 747, * Airbus 340, * McDowell MD-11
<b>Class IV High maneuverability airplanes such as:</b> * Fighter / interceptor * Attack * Tactical reconnaissance * Observation * Trainer for Class IV	* Lockheed F-22 * McDowell F-15E * McDowell RF-4 * Lockheed SR-71 * Northrop T-38	FAR 23 aerobatic category airplanes	* Pitts Special, * Sukhoi Su-26M

Fig. 15 Definition of Airplane Classes.

For the flight phases, both aircraft were analyzed to perform under cruise conditions, so the Category B flight phase was chosen for both. The criterion for this category is listed below in Figure 16, found in Roskam [6].

MIL-F-8785C	Suggested Civilian Equivalent: VLA, FAR 23 and FAR 25
<b>Category B:</b> Those non-terminal flight phases that are normally accomplished using gradual maneuvers and without precision tracking, although accurate flight-path control may be required. Included in this category are:	
a) Climb (CL)	Various climb segments
b) Cruise (CR)	Various cruise segments
c) Loiter (LO)	Flight in holding pattern
d) In-flight refuelling (tanker) (RT)	None as yet
e) Descent	Various descent segments
f) Emergency descent (ED)	Emergency descent
g) Emergency deceleration (DE)	None
h) Aerial delivery (AD)	Parachute drop

Fig. 16 Definition of Flight Phase Categories.

With the class and phase category decided for each aircraft, the next step for finding their flying quality level was to analyze their damping ratios and rise times. The system transfer function equations were utilized, with the equation of the denominator being:

$$s^2 + 2w_n\xi s + w_n^2 \quad (26)$$

This yielded damping ratios for systems with complex roots. For systems with real roots and spiral and roll modes, the time constant and the time to double the amplitude were used. Their equations are:

$$\tau = \frac{1}{root} \quad (27)$$

$$\tau_{2amp} = \ln(2) * \tau \quad (28)$$

The Learjet-25 Phugoid, short-period, Dutch roll, spiral, and roll damping ratios were calculated first using the roll rate to aileron deflection input transfer function and pitch rate to elevator deflection input transfer function. Its spiral and roll modes' rise times were found from the transfer function MATLAB codes. Table 4 and Table 5 shows the Learjet's frequencies and ratios for the modes.

Mode	$w_n(\text{rad/s})$	$\xi$
Phugoid	0.092	0.034
Short Period	3.51	0.44
Dutch Roll	1.77	0.079
Spiral	$\tau(\text{s})$	3610
Roll	$\tau(\text{s})$	0.41

**Table 4 Learjet-25 Configuration 1 Frequency, Damping Ratios, and Rise Times**

Mode	$w_n(\text{rad/s})$	$\xi$
Phugoid	0.094	0.0277
Short Period	3.05	0.44
Dutch Roll	1.46	0.073
Spiral	$\tau(\text{s})$	DNE
Roll	$\tau(\text{s})$	0.851

**Table 5 Learjet-25 Configuration 2 Frequency, Damping Ratios, and Rise Times**

The spiral mode for configuration two was unstable resulting in no spiral rise time.

A different approach was taken for the F-4 longitudinal modes. The F-4 had a longitudinal transfer function of real roots ratios so the eigenvalues for the short period was used to calculate frequency and damping ratio, similar to Homework 5 the equations shown below.

$$w_n = \sqrt{\text{real}^2 + \text{imaginary}^2} \quad (29)$$

$$\xi = \frac{1}{w_n} \quad (30)$$

The eigenvalues for the mode were  $-6.29e-01 \pm 2.78e+00i$ . The time constants for the other modes are also shown below in Table 6 and Table 7.

Mode	$w_n(\text{rad/s})$	$\xi$
Short Period	2.85	0.221
Dutch Roll	2.4	0.048

**Table 6 F-4 Frequency and Damping Ratios**

Mode	$\tau(\text{s})$
Phugoid	25.9
Spiral	76.3
Roll	74.7

**Table 7 F-4 Rise Times**

For the Phugoid damping requirements, the Learjet-25 performed at level II and the F-4 at level II using 17, found in Roskam [6].

MIL-F-8785C	VLA, FAR 23 and FAR 25
Level I: $\zeta_{ph} \geq 0.04$	No requirement
Level II: $\zeta_{ph} \geq 0$	No requirement
Level III: $T_{2_{ph}} \geq 55 \text{ sec}$	No requirement

**Fig. 17 Phugoid Damping Requirements.**

Looking at the short periods and Figure 18, the Learjet-25 performed at level I and the F-4 at level II, found in Roskam [6].

Level	Category A and C Flight Phases			Category B Flight Phases		
	Minimum	Maximum		Minimum	Maximum	
Level 1*	0.35	$\leftarrow \zeta_{sp} \rightarrow$	1.30	0.30	$\leftarrow \zeta_{sp} \rightarrow$	2.00
Level 2	0.25	$\leftarrow \zeta_{sp} \rightarrow$	2.00	0.20	$\leftarrow \zeta_{sp} \rightarrow$	2.00
Level 3	0.15 **	$\leftarrow \zeta_{sp} \rightarrow$	no maximum	0.15 *	$\leftarrow \zeta_{sp} \rightarrow$	no maximum

\* For VLA, FAR 23 and FAR 25 :  $\zeta_{sp}$  must be heavily damped

**Fig. 18 Short Period Damping Ratio Limits.**

For the lateral modes, the Dutch roll damping ratio showed the Learjet-25 at level II and the F-4 also at level II based on Figure 19, found in Roskam [6].

**Mil-F-8785C**

Level	Flight Phase Category	Airplane Class	Min. $\zeta_d$ *	Min. $\zeta_d \omega_{n_d}$ * rad/sec	Min. $\omega_{n_d}$ rad/sec
Level 1	A (Combat and Ground Attack)	IV	0.4	-	1.0
	A (Other)	I and IV	0.19	0.35	1.0
		II and III	0.19	0.35	0.4**
	B	All	0.08	0.15	0.4**
		I, II-C and IV	0.08	0.15	1.0
	C	II-L and III	0.08	0.10	0.4**
Level 2	All	All	0.02	0.05	0.4**
Level 3	All	All	0	-	0.4**

\* The governing requirement is that which yields the largest value of  $\zeta_d$ .

Note : For Class III  $\zeta_d = 0.7$  is the maximum value required.

\*\* Class III airplanes may be excepted from these requirements, subject specific approval.

**Civilian Requirements:**

FAR 23 and VLA:  $\zeta_d > 0.052$  with controls – free and controls – fixed

FAR 25:  $\zeta_d > 0$  with controls – free and must be controllable without exceptional pilot skills

**Fig. 19 Minimum Dutch Roll Undamped Natural Frequency and Damping Ratio Requirements.**

The time to double the amplitude in spiral mode was 52.9s for the F-4 and 2500s for the Learjet-25 for configuration 1. Using Figure 20, they both perform at level I, as described in Roskam [6].

Flight Phase Category	Level 1	Level 2	Level 3
A and C	$T_{2_s} > 12$ sec	$T_{2_s} > 8$ sec	$T_{2_s} > 4$ sec
B	$T_{2_s} > 20$ sec	$T_{2_s} > 8$ sec	$T_{2_s} > 4$ sec

**Fig. 20 Minimum Time to Double the Amplitude in the Spiral Modes.**

The roll time constants are shown in Figure 21. The roll time constants of the aircraft fall under level I, as shown in Roskam [6].

Flight Phase Category	Airplane Class	Level 1	Level 2	Level 3
A	I and IV	$T_r \leq 1.0$ sec	$T_r \leq 1.4$ sec	$T_r \leq 10.0$ sec
	II and III	$T_r \leq 1.4$ sec	$T_r \leq 3.0$ sec	$T_r \leq 10.0$ sec
B	All	$T_r \leq 1.4$ sec	$T_r \leq 3.0$ sec	$T_r \leq 10.0$ sec
C	I, II-C and IV	$T_r \leq 1.0$ sec	$T_r \leq 1.4$ sec	$T_r \leq 10.0$ sec
	II-L and III	$T_r \leq 1.4$ sec	$T_r \leq 3.0$ sec	$T_r \leq 10.0$ sec

**Fig. 21 Maximum Allowable Roll Mode Time Constant.**

With pilot performance and safety being a major factor in handling quality, the aircraft is stated to perform at Level II since it requires more action from the pilot to navigate possible deficiencies than at Level I. According to the

Cooper-Harper pilot rating, at level II, the pilot rates it from 4-6 with moderate pilot compensation to extension pilot compensation to fly. Figure 20 shows more detail about what level II all entails, shown in Roskam [6].

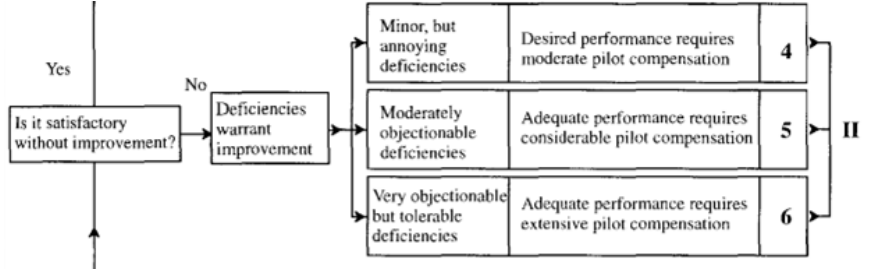


**Fig. 22 Cooper-Harper Pilot Rating Scale.**

Comparing the calculated levels to other literature on other fighter jets and high-performance aircraft, they also fell on Level II, agreeing with the findings from Figure 23, as shown in Peahl [5].

Flight Config.	Pilot Rating	HQ Level
A	3,3	1
B	4,5	2
C	2,3	1
D	5	2

**Fig. 23 Flight Phase and Handling Qualities of High Performance Aircraft.**

Fighters and jets were analyzed with their result showing that an aircraft in phase B was typically rated at a handling quality of 2 and a pilot rating of 4-5.

## B. Controllers

### 1. F-4 Pitch/Roll-Hold Controllers

The F-4 prioritizes maneuverability with its controllers, allowing the aircraft to make high-precision, aggressive maneuvers common in Class A flight, found in Roskam [6]. The controllers were tuned using methods detailed above, changing  $K_p$ ,  $K_I$ , and  $K_d$  to produce the desired effect, creating a fast-acting response with low oscillation.

**Pitch Hold Controller** The Pitch Controller is constructed using Simulink, with a negative feedback loop, and using a PID controller with a low-pass filter as described previously.

**Pitch Hold Loop Transfer Function** Using Eq. 25 found above, the transfer function for the full closed loop can be derived to be:

$$\frac{\Theta(s)}{\Theta_c(s)} = \frac{(K_p + \frac{K_i}{s} + \frac{K_d s}{\tau s + 1}) \frac{\Theta(s)}{i_h(s)}}{1 + (K_p + \frac{K_i}{s} + \frac{K_d s}{\tau s + 1}) \frac{\Theta(s)}{i_h(s)} e^{-T_d s}} \quad (31)$$

This equation described how the pitch of the system ( $\Theta$ ), reacts to the pitch input ( $\Theta_c$ ). With each variable displayed in Table 8.

Variable	Value
$K_p$	-0.4
$K_I$	-0.05
$K_d$	-0.05
$\tau$	$5 \times 10^{-6}$
$T_d$	0.005 s

**Table 8 F-4 Pitch Hold Loop Values**

Comparing the frequency responses of the original and controlled systems, Figure 24 is produced. The plot demonstrates that the controller reduces the amplitude and phase of the system, making the aircraft more controllable.

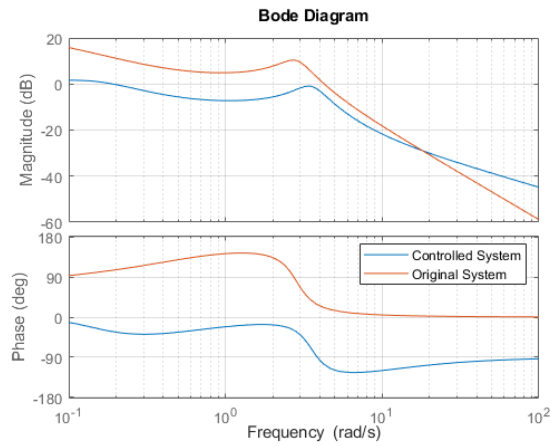


**Fig. 24 Frequency Responses of Pitch Controller**

Graphing the poles of the system shows a similar result, making the original poles more negative, increasing stability. As shown in Figure 25.

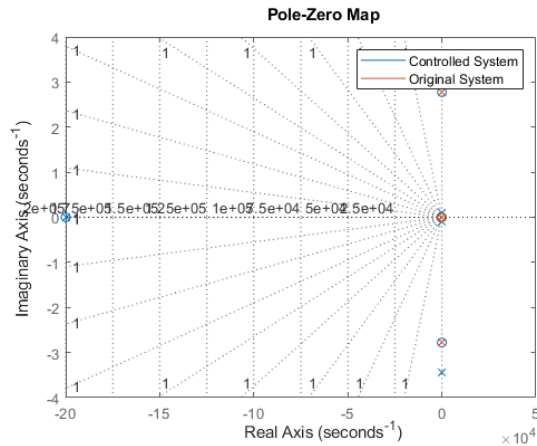


**Fig. 25 Root Locus of Pitch Controller**

Roll Hold Controller

**Roll Hold Loop Transfer Function** Using a similar method, as described above, the transfer function for the closed loop can be found to be:

$$\frac{\Phi(s)}{\Phi_c(s)} = \frac{(K_p + \frac{K_i}{s} + \frac{K_d s}{\tau s + 1}) i_h(s)}{1 + (K_p + \frac{K_i}{s} + \frac{K_d s}{\tau s + 1}) \frac{\Phi(s)}{i_h(s)} e^{-T_d s}} \quad (32)$$

Variable	Value
$K_p$	0.5
$K_I$	0.05
$K_d$	0.06
$\tau$	$5 \times 10^{-10}$
$T_d$	0.005 s

**Table 9 F-4 Roll Hold Loop PID Gains**

Using the same method as the pitch-hold controller, the frequency responses and root loci for the systems are shown in Figures 26 and 27.

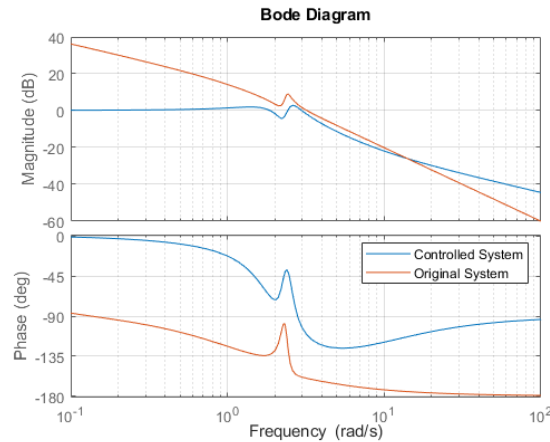


**Fig. 26 Frequency Responses of Roll Controller**

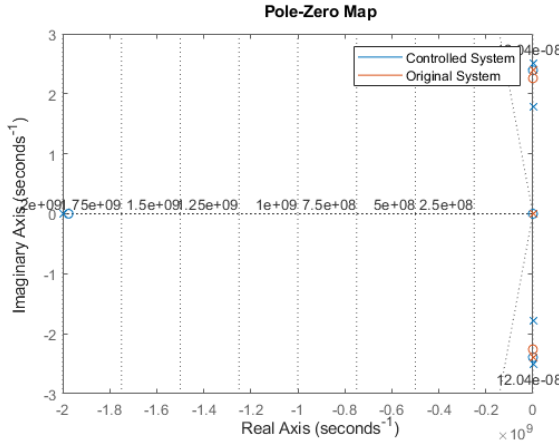


**Fig. 27 Root Locus of Roll Controller**

**Controller Evaluation** Evaluating the controllers using the criteria described earlier, allows for a quantitative analysis of the effectiveness of the controller. The F-4 controllers show good performance with minimal overshoot and an excellent rise and settling time, shown in Table 10.

Controller	Rise Time (0-63%)	Settling Time (5%)	Overshoot (%)
Pitch Controller	1.1364 s	1.3443 s	1.181
Roll Controller	1.1302 s	1.3101 s	1.4461

**Table 10 F-4 Controller**

## 2. Learjet-25 Pitch/Roll-Hold Controllers

The Learjet-25 prioritized comfort and stability for its controllers, as needed for Class B & C Flight [6]. The same PID controller was used for both configurations of the jet to compare how differing trim states may require different gain sets to maintain stability and performance.

Pitch Hold Controller (Configuration 1) The first configuration (Configuration 1) represents a more stable trim state. Two pitch-hold controllers were developed using the configurations provided in Berger [8]. Each configuration presents unique trim and stability characteristics, necessitating separate evaluation. The feedback loop employed the same architecture as the F-4 pitch controller, shown in Figure 28. The controller gains used for both pitch controllers are shown in Table 11.

Variable	Value
$K_p$	-8
$K_I$	-0.08
$K_d$	-1.5

**Table 11 Learjet-25 Pitch Hold Loop PID Gains**

Figure 29 shows the Bode plots comparing the open-loop and closed-loop pitch dynamics for both configurations. For Configuration 1, the controller slightly increases system gain at low frequencies while maintaining the overall frequency response shape. This suggests that the controller improves command authority without drastically altering the system's natural dynamics. The phase behavior is also mostly preserved, indicating that the controller does not significantly degrade phase margin or introduce instability.

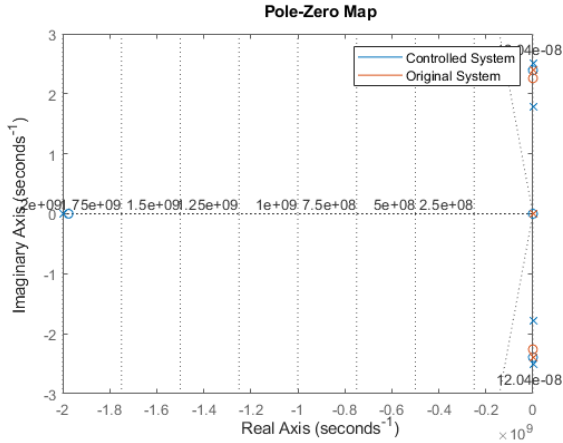


**Fig. 28 Pole-zero Plot for F-4 roll hold controller geometry**

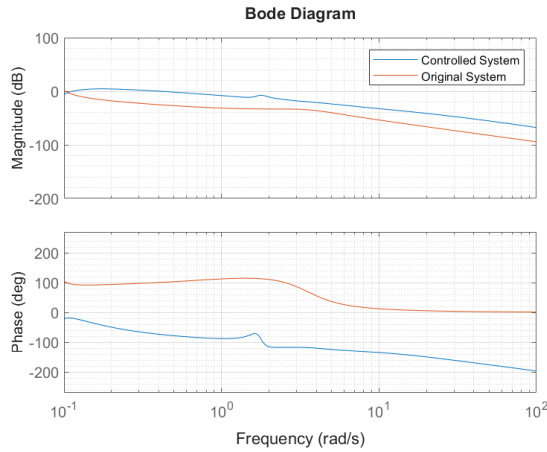


**Fig. 29 Bode plot comparison for Learjet-25 Pitch Hold Controllers**

The pole-zero diagram for the closed-loop system (Figure 28) reveals that the poles have shifted further into the left-half plane compared to the uncontrolled system. This movement indicates increased stability, as the system's eigenvalues exhibit more negative real parts. The pole placement confirms that the controller improves damping while keeping the system response predictable.

#### Roll Hold Controllers (Configuration 1)

The same PID gains were applied to the roll-hold controllers, as listed in Table 12. Figure 30 shows the Bode plots for the roll axis in both configurations. Configuration 1 maintains good roll stability and responsiveness with minimal overshoot, validating the controller design under this trim condition.

Variable	Value
$K_p$	-8
$K_I$	-0.08
$K_d$	-1.5

**Table 12 Learjet-25 Roll Hold Loop PID Gains**

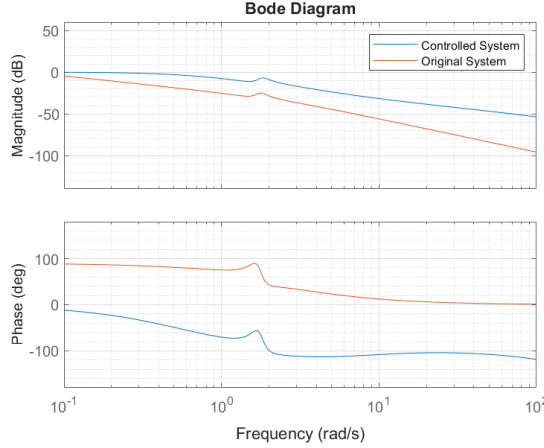


**Fig. 30 Bode plot comparison for Learjet-25 Roll Hold Controllers**

**Configuration 2 Frequency Response and Stability** Configuration 2 uses the exact same PID gains and feedback geometry as Configuration 1. However, despite this shared controller design, it demonstrates significantly different frequency response behavior. Figure 31 shows that the pitch loop for Configuration 2 becomes more dynamic, with increased gain and signs of marginal damping at mid-frequencies. The associated pole-zero plot (Figure 32) shows poles migrating closer to the imaginary axis, indicating reduced stability margins.

Most notably, the roll response becomes completely unstable. The poles move into or near the right-half plane, resulting in unbounded response to inputs. This is a direct consequence of applying the same fixed-gain controller to a different trim condition without adaptation. The change in aircraft dynamics due to configuration, trim state, or flight regime can alter the linearized model significantly enough that a controller tuned for one regime becomes ineffective or destabilizing in another. This result highlights the fundamental limitation of fixed-gain control: what stabilizes one trim condition may fail for another, necessitating gain scheduling or adaptive control strategies for robust performance.

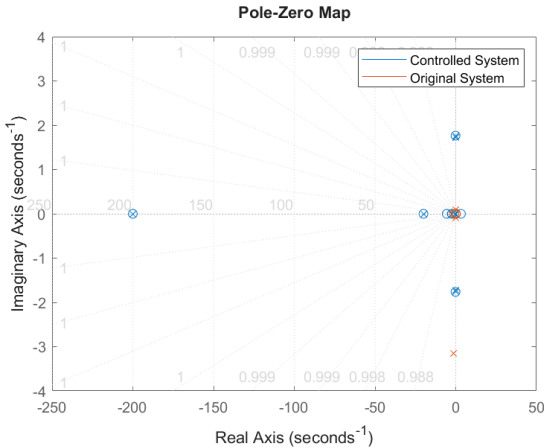


**Fig. 31 Bode plot for Configuration 2 Pitch Hold Response**

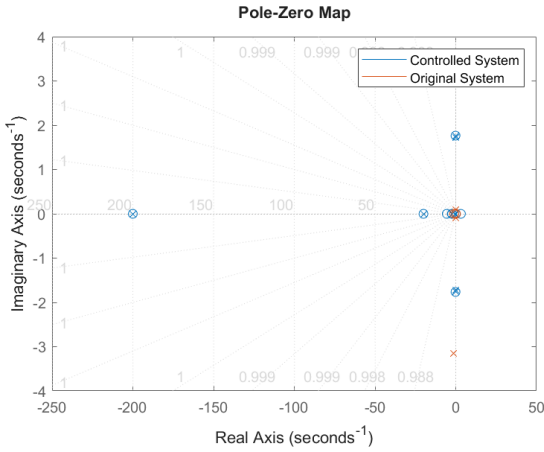


**Fig. 32 Pole-zero diagram for Configuration 2**

**Step Response Comparisons** To further understand the system behavior, step responses for each controller and configuration are shown in Figures 33 and 34. These plots illustrate time-domain characteristics like rise time, overshoot, and settling, supporting the quantitative metrics shown in Table 13.

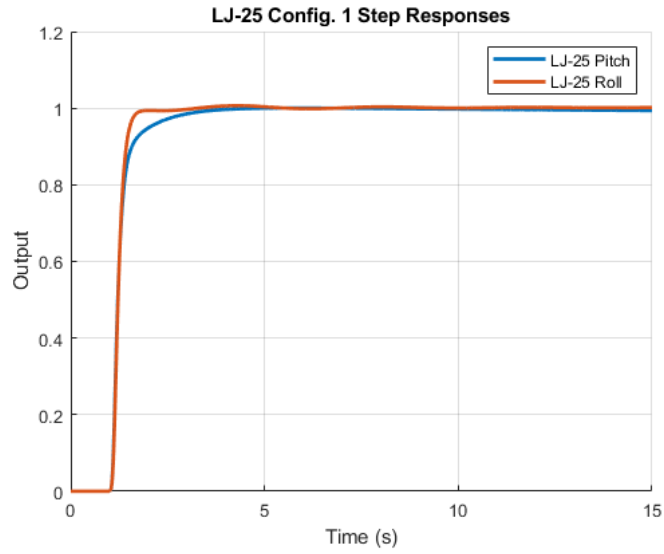


**Fig. 33 Pitch and Roll Response for Learjet Config. 1**

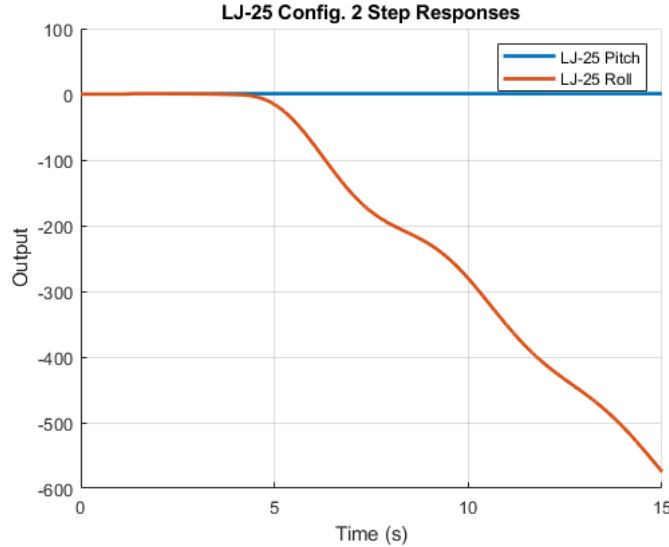


**Fig. 34 Pitch and Roll Response for Learjet Config. 2**

**Controller Evaluation** Table 13 summarizes the performance metrics for all controller/configuration pairs, including rise time, settling time, and percent overshoot.

Controller	Rise Time (0-63%)	Settling Time (5%)	Overshoot (%)
Config. 1 Pitch Controller	1.2658 s	1.7818 s	2.1593
Config. 1 Roll Controller	1.2658 s	1.5378 s	0.054325
Config. 2 Pitch Controller	1.2557 s	9.2487 s	5.2267
Config. 2 Roll Controller	0.3243 s	—	$\infty$

**Table 13 Evaluations of PID Controllers on Learjet-25 Models**

The two Learjet-25 configurations exhibit noticeably different behavior under identical PID control, reinforcing the critical importance of tuning for specific flight conditions. Configuration 1 demonstrates well-damped, stable responses in both pitch and roll channels, with low overshoot and fast settling times. This indicates that the controller is well-matched to the dynamics of that particular trim condition.

Configuration 2, however, reveals the pitfalls of applying a one-size-fits-all control strategy. Its pitch controller produces higher overshoot and significantly longer settling time, while its roll controller becomes unstable. These outcomes reflect how changes in trim condition and aircraft dynamics alter the underlying system behavior, rendering previously tuned controllers ineffective. As such, successful implementation across multiple trim states requires either retuning, gain scheduling, or adaptive control methods tailored to each configuration.

### C. Simulator

**Nonlinear Flight Simulation of the F-4 Phantom** To further evaluate the control system performance under realistic flight conditions, a nonlinear flight dynamics simulation of the F-4 Phantom was developed. Unlike linearized models used for control design and frequency analysis, a nonlinear simulator captures the full six-degree-of-freedom (6-DOF) motion of the aircraft, including aerodynamic nonlinearities, coupled rotational and translational dynamics, and actuator limits.

**Model Overview** The nonlinear model includes translational dynamics in the body frame ( $u, v, w$ ), rotational dynamics ( $p, q, r$ ), and Euler angle kinematics ( $\phi, \theta, \psi$ ). Force and moment equations are driven by aerodynamic coefficients that

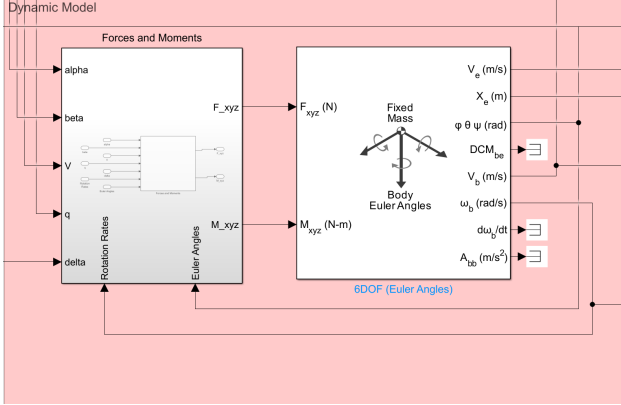


**Fig. 35 Nonlinear Dynamic Model for F-4**

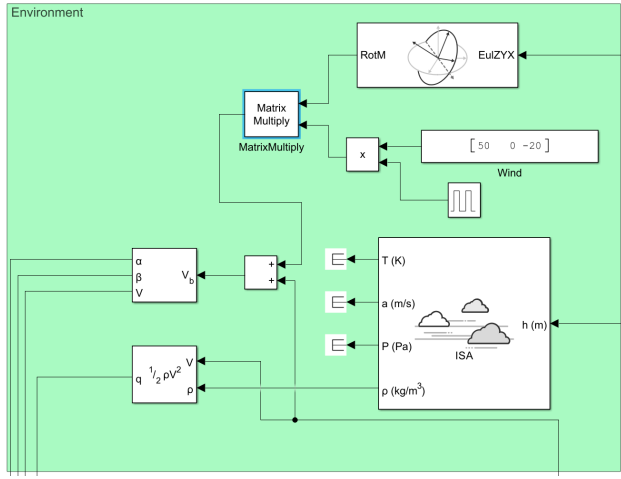


**Fig. 36 Nonlinear Atmospheric Model for F-4**

are functions of angle of attack ( $\alpha$ ), sideslip ( $\beta$ ), and control surface deflections. Engine thrust, gravity, and control input limits are also included to model realistic flight behavior.

**Implementation** The simulator was developed in Simulink and is based on the full rigid-body force and moment equations governing aircraft motion. Aerodynamic coefficients were sourced from Roskam [6]. The control system inputs are provided by the previously developed PID controllers. Actuator dynamics are modeled using both rate-limiters and saturation blocks to replicate physical constraints.

To account for altitude effects on aircraft performance, a standard atmosphere block from the Simulink aerospace toolbox is incorporated as shown in Figure 36. This enables dynamic adjustments in air density and pressure, ensuring more accurate modeling of forces and control effectiveness at altitude. The simulation adds in a wind gust feature to show the effects of wind on the aircraft and how the controller adjusts for it. The simulation is initialized near a stable trim point, providing a baseline from which small perturbations can be introduced and managed by the controller. This approach facilitates control analysis while ensuring the system remains near a controllable operating region.

**Pitch-Axis Stability and Disturbance Rejection** To validate the closed-loop pitch dynamics beyond the linear envelope, the nonlinear model implemented a wind gust model to add disturbances and analyze controller response.

- **Initial pitch upset:** The gust generated an immediate  $4.8^\circ$  nose-up excursion and a spike in pitch rate of  $12 \text{ deg/s}$ . Without control, the model diverged in under  $6 \text{ s}$ .
- **Controller response:** The PID loop arrested the pitch-rate peak within  $0.35 \text{ s}$  and returned the attitude to within  $\pm 0.7^\circ$  of trim after  $1.8 \text{ s}$ . Integral action removed the residual bias introduced by the gust in  $\approx 3 \text{ s}$  with no

secondary overshoot.

- **Actuator usage:** Elevator deflection stayed inside  $\pm 8.6^\circ$ , well below the  $\pm 15^\circ$  saturation limit, confirming margin for harsher turbulence or maneuver commands.

These results reinforce the linear analysis: the controller provides strong damping in the short-period mode and maintains command authority under combined aero-structural coupling and realistic atmospheric disturbances. Importantly, actuator headroom remains, indicating robustness against larger upsets or unmodelled non-linearities.

#### D. Longitudinal Pitch Aircraft Upsets and Possible Recovery with Thrust

Control surface failure effects are a subfield of dynamics that is an area of interest as it pertains to possible safety improvements and knowledge. Safety within the aerospace field is of great importance. This can be seen through intense scrutiny in certification, maintenance schedule for every part down to the smallest of screws, and aircraft checks between every flight. Government regulations call loss of control or unusual attitudes of an aircraft, "Airplane Upsets" [7]. Aircraft upsets can be caused by control surface failures that effect the aircraft dynamics in both the lateral and longitudinal directions. In this report, a single control surface failure will be analysis for a single trim point. The focus is on elevator control failure and if a throttle input could compensate for the "Airplane Upset" as described in the Airplane Flying Handbook (FAA-H-8083-3C) which are shown in table 14.

Airplane Upset Condition	
1	Pitch Attitude Greater than $25^\circ$ , nose up
2	Pitch Attitude Greater than $10^\circ$ , nose down
3	Bank Angle Greater than $45^\circ$
4	Within the above parameters, but flying at airspeed inappropriate for the conditions

Table 14 FAA Regulation Policy on Airplane Upset [7]

The linear longitudinal models for the F-4 and Learjet-25 will be used with the control inputs  $\delta_e$  and  $\delta_T$ : the elevator deflection angle and the throttle inputs. The longitudinal model only uses conditions one and two from Table 14. With these definitions, previous research about pitch failure in similar aircraft types can be used to compare as long as the reactivity is similar with what was generated in the generated responses and plots. Using elevator failure with thrust compensation becomes difficult as the introduction of thrust causes a change in the trim conditions. The base exploratory idea for the aircraft to become stable using thrust compensation comes from using the system transfer functions to achieve equilibrium of the pitch rate as shown in Equation 33.

$$\frac{q}{\delta e} - \frac{q}{\delta t} = 0 \quad (33)$$

The notion is that as the pitch rate change approaches zero the aircraft should achieve steady state flight. However this is flawed as the forces and moments are reliant on dynamic pressure which is effected by the body velocity of the aircraft. Remembering that the body-axis velocity has the components of  $u$ ,  $v$ , and  $w$ , the state space models have a minimum of one of these components non-constant when trying to compensate for elevator failure with thrust. Thus as the dynamic pressure changes with enough difference the aircraft leaves the chosen trim state and a new model or trim state is required:

$$V_B = \sqrt{u^2 + v^2 + w^2} \quad \bar{q} = \frac{1}{2} \rho V_B^2 \quad (34)$$

This is highlighted by the mathematical derivation between linear and nonlinear systems as discussed in Section III, and explored in Appendix A of Section VI. This process provided by Roskam [6] can applied to both aircraft, thus it will be that the fundamental changes in the dynamic pressure will not make thrust compensation possible. Additionally, variations within the state space models for the different aircraft exist as well where the Learjet 25 and F-4 fighter will have different frequencies of response to the failure with thrust. Both aircraft belong to separate class types The Learjet 25 is a Class II, medium transport general aircraft, and the F-4 fighter is a Class IV, high maneuverability aircraft. The F-4 state-space model used does not have a thrust input, so analysis for the F-4 uses previous AIAA research and National Transportation Safety Board (NTSB) incident reports to show why it is not feasible. The infeasibility is partly due to the fact that fighters generate a higher magnitude of forces and moments which the thrust will not be able to

compensate. The Learjet 25 state space model can be mathematically analyzed in order to determine that a pitch aircraft upset due to elevator failure and possible thrust usage for recovery is not possible and to support why the linearized model is so effected.

### 1. The Learjet 25

To determine if the Learjet can compensate for a loss in elevator control with thrust, a study of the longitudinal model was initially done. If the goal is to have the aircraft have an elevator-induced response and for the thrust to subsequently return it back to a steady state then the the state equation,  $\dot{x} = f(x, u)$  will need to equate to zero:

$$\begin{bmatrix} \dot{\theta} \\ \dot{w} \\ \dot{q} \\ \dot{\phi} \\ \dot{\psi} \end{bmatrix} = A \begin{bmatrix} u \\ w \\ q \\ \theta \\ \phi \end{bmatrix} + B \begin{bmatrix} \delta_e \\ \delta_T \end{bmatrix} \quad (35)$$

For the case of the Learjet 25 the state space model from Berger[8] needs to be of form:

$$\begin{bmatrix} \dot{\theta} \\ \dot{w} \\ \dot{q} \\ \dot{\phi} \\ \dot{\psi} \end{bmatrix} = \begin{bmatrix} X_u & X_w & X_q - W_0 & -g \cos \Theta_0 \\ Z_u & Z_w & Z_q - U_0 & -g \sin \Theta_0 \\ M_u & M_w & M_q & 0 \\ 0 & 0 & 1 & 0 \end{bmatrix} \begin{bmatrix} u \\ w \\ q \\ \theta \end{bmatrix} + \begin{bmatrix} X_{\delta_e} & X_{\delta_T} \\ Z_{\delta_e} & Z_{\delta_T} \\ M_{\delta_e} & M_{\delta_T} \\ 0 & 0 \end{bmatrix} \begin{bmatrix} \delta_e \\ \delta_T \end{bmatrix} \quad (36)$$

Using the outputs  $u, w, q = 0$ , and  $\theta$  along with  $\delta_e$  and  $\delta_T$  as a system means that the throttle and elevator angle inputs effect the forces in the X and Z axis directions and the pitching moment differently within the system. The differences in forces and moments come from the thrust-throttle relationship and influences from the velocity. A change in the velocity components,  $u$  and  $w$ , occurs which then cause a dynamic pressure change that then effect the forces and moments removing the system far from the trim state as the perturbations are too large and making the aircraft uncontrollable and the state space model no longer valid.

### 2. The F-4

The first issue in analyzing the state space model of the F-4 fighter from Roskam [6] is that the model does not provide the ability for thrust compensation in its current trim condition. Thus real-world application and research on similar class IV aircraft with pitch failure is required. Two key reports that will be used is one that involves the X-15 3-65 from Orr[4] and another that evaluated the handling quality evaluations for reduced pitch and roll damping scenarios with an F-18 fighter and references to other adaptive systems of the F-94A, X-15, F-16, and the F-15 by Hanson[2]. Hanson[2] uses nonlinear dynamic inversion (NDI) controllers to produce gradient-based results for the pitch and roll axis parameters, while Orr[4] is an analysis of a fatal accident that took place in 1967. Starting with the adaptive control model from Hanson[2] the state equation used is:

$$\dot{x}(t) = Ax(t) + B(u(t) - \sigma(t)) \quad (37)$$

Where  $\sigma(t)$  is a scalar, time-varying uncertain disturbance; something in which is not taken into consideration with the models of this paper. This is a more complex version of the basic state space model, Equation 15, used in the linear system theory considered in Section III.C. Meaning that Hanson[2] is also taking additional issues in consideration. Though similar to the topic of the F-4 and Learjet 25 the pitch axis implementation also uses  $\frac{q}{r_q}(s)$  where  $r_q$  is the scalar input. Comparatively, the fighter analysis also calculates the input as a reference signal as a function of the pilot longitudinal stick, an error signal and an adaptive control command. One of the results that is impossible to generate with theory alone is pilot ratings between healthy aircraft and failure scenarios as seen below in Figure 37.

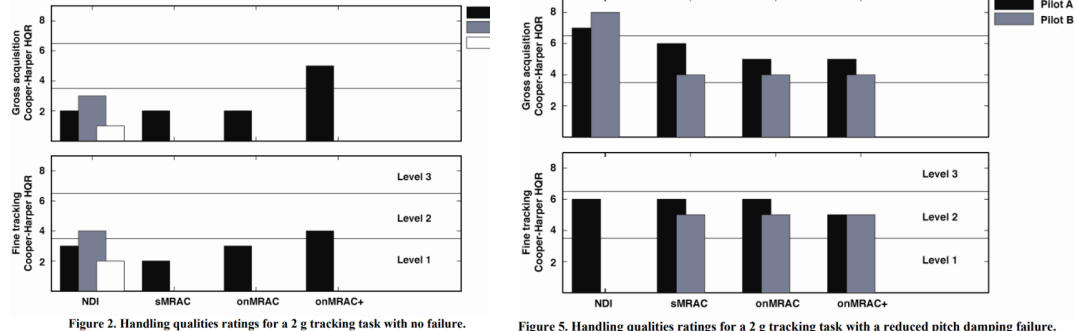


Figure 2. Handling qualities ratings for a 2 g tracking task with no failure.

(a) Before Pitch Failure

Figure 5. Handling qualities ratings for a 2 g tracking task with a reduced pitch damping failure.

(b) After Pitch Failure

**Fig. 37 Cooper-Harper Scale Ratings Before and After Pitch Failure Results[2]**

The results of this showed that there was a great increase of handling on the Cooper-Harper Scale in which there was a minimum of a two-level increase and a maximum of a five-level increase up to a maximum of a level eight scoring during a reduced pitch damping failure. The Cooper-Harper Scale is used for pilot ratings for characteristics of the aircraft performance and can be viewed in Figure 39.

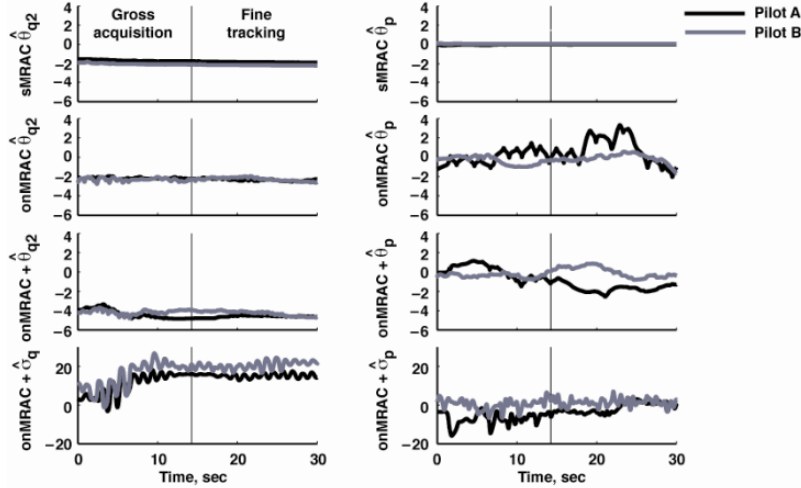


Figure 7. Adaptive parameters during the 2 g tracking task with a reduced pitch damping failure.

**Fig. 38 Dynamic Adaptive Parameter Results with Reduced Pitch Damping Failure[2]**

In which the results in Figure 38 were based off gross acquisition movement versus the fine tracking handling. It was found that there was little complexity when there was only pitch failure but the roll axis gradients needed to be close to zero ideally. The findings did show that the roll axis would have a roll during pitch failure for fighters when reduced pitch damping was involved [2]. This can be seen additionally in the X-15 incident of 1967. During the incident the flight control system malfunctioned due to electrical and experiment package failure effectively interrupting the pilot access to the reaction control system. This lead to hardover failures and complete disengagement of the stability augmentation of the roll, pitch and yaw axis [4]. Wherein once more failure occurs not only in pitch but associated with the other axis due to the moments and forces. This can be seen in the X-15 report with a reproduced linear system:

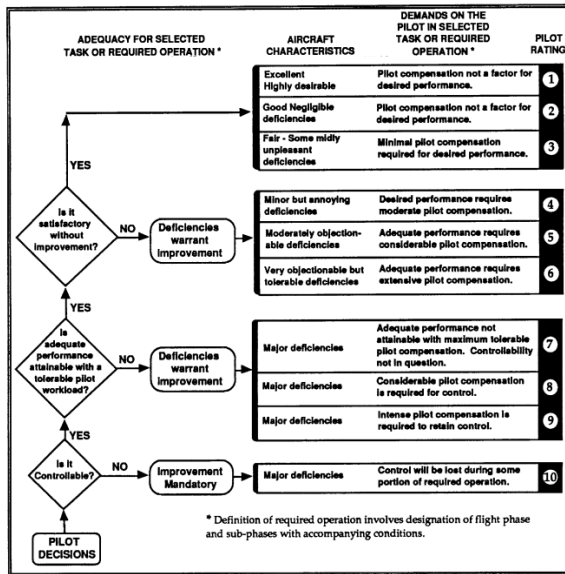


Figure 1: The Cooper-Harper Pilot Rating Scale

Fig. 39 Cooper-Harper Scale [3]

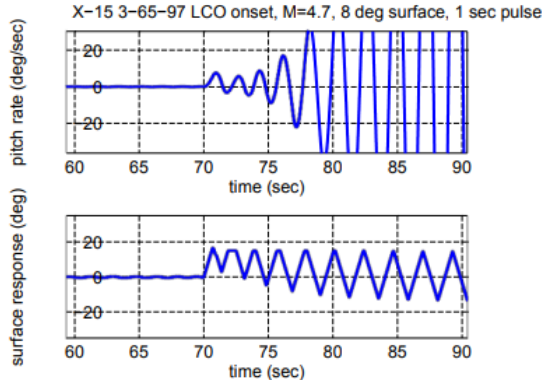


Figure 5.0-1. Flight 3-65 Divergent LCO Reproduced in Nonlinear Simulation ( $M=4.7$ ,  $q=390 \text{ psf}$ )

Fig. 40 1967 X-15 Failure Stability Simulation by Orr[4]

This is because of intense surface responses of class IV aircraft, which is shown by the x-15 crash results of Figure 40 and supported by the response in the bode plot response of Figure 11 and Figure 12 which shows similar sensitive reactivity leading to a failure in which thrust cannot compensate. Overall the analysis and research conclude that the aircraft does not have the ability to circumvent a pitch failure due to the interoperability of the elevator occurs with thrust. This is due to the fact that the elevator deflection has a very different effect on the forces and moments on the aircraft than a change in throttle. This means the throttle cannot be used to replace elevator deflection.

#### E. Initial Conditions and Test Cases

Simulations were run at a representative trim condition: level flight at 25,000 ft and 450 knots. Initial pitch and roll perturbations were applied to assess controller recovery. Additional test cases included steady turns and step changes in pitch rate command.

## VI. Conclusion

This describes the methods used to create both linear and nonlinear models of specific aircraft, the process used to create a PID controllers for those models and how the models and controllers were validated. The models were created based on information about the F-4 and Learjet 25. The F-4 had one linear and one nonlinear model and the Learjet 25 had two linear models. These models were validated using doublet responses and Bode plots. The doublet responses were used to confirm that the models would react appropriately to inputs. Doublets were used on both linear and non-linear models while Bode plots could only be used to validate the linear models. Bode plots show the frequency response of both aircraft and that information was used determine the model's sensitivity to different control surface inputs.

The linear models and frequency response information were then used to create a series of PID controller systems. These controllers were validated by comparison between different flight conditions, the stability of their corresponding linear models, and the frequency response results from the Bode plots.

finally, an elevator failure analysis of both aircraft was conducted. This analysis attempted to determine if elevator failure can be compensated a change in thrust. Through examination of existing literature and analysis of the model. It was found that neither the F-4 Phantom nor the Learjet 25 could compensate for elevator failure through thrust compensation. This is due to two facts. First, the situations where failure occurred often including more than one control surface. Second, The fact that the thrust affects the states of the aircraft in different proportions than the elevator deflection leads to out of control states even if it tries to control on of the states.

## Appendix A: Non-linear to Linear Derivation

The derivation of the longitudinal and lateral state space matrices begins with the 6-DOF equations of motion and the kinematic equation, which are presented above as Equations 1-10. These equations need to be linearized to be expressed in matrix form. To do this, each state in the equation needs to be replaced with an addition of states, as shown in Equation 38, where X is the total value of the state,  $X_1$  is the steady-state or trim value of the state, and x is the perturbed value of the state.

$$X = X_1 + x \quad (38)$$

For the state U, the equation becomes  $U = U_1 + u$ . When equation 38 is applied to equation 1, it becomes Equation 39, shown below.

$$m(\dot{U}_1 + \dot{u}) = F_{x,1} + f_x - mg(\sin(\Theta_1 + \theta)) + m((R_1 + r)(V_1 + v) + (Q_1 + q)(W_1 + w)) \quad (39)$$

The next step is to expand all the terms in equation A.5 and apply the three following assumptions. The  $\sin(X_1 + x)$  term is expanded using a trigonometric identity to be  $\sin(X_1)\cos(x) + \cos(X_1)\sin(x)$

1. Terms that are in the general steady state equation of motion can be removed because the equation of motion is already satisfied
  2. Perturbed terms are small, so the multiplication of two perturbed terms results in number that is approximately equal to zero
  3. All perturbed angles are small, so the small angle assumption can be applied which is  $\sin(x) \approx x$  and  $\cos(x) \approx 1$
- The assumptions applied to equation 39 are shown below. These simplifications result in equation 40

$$m\ddot{U}_1^0 + m\dot{u} = F_{x,1}^0 + f_x + -mg(\sin(\Theta_1^0) + \theta \cos(\Theta_1)) + m(R_1 V_1^0 + V_1 r + R_1 v + r v^0 + Q_1 W_1^0 + W_1 q + Q_1 w + q w^0) \quad (40)$$

$$m\dot{u} = f_x + -mg\theta \cos(\Theta_1) + m(V_1 r + R_1 v - W_1 q - Q_1 w) \quad (41)$$

This process is repeated for Equations 1-9 using the same assumptions, to obtain Equations 41-49

$$m\dot{v} = f_y + mg(-\theta \sin \Phi_1 \sin \Theta_1 + \phi \cos \Phi_1 \cos \Theta_1) - mU_1 r - mR_1 u + mW_1 p + mP_1 w \quad (42)$$

$$m\dot{w} = f_z - mg\theta \cos \Phi_1 \sin \Theta_1 - mg\phi \sin \Phi_1 \cos \Theta_1 + mU_1 q + mQ_1 u - mV_1 p - mP_1 v \quad (43)$$

$$I_{xx}\dot{p} - I_{xz}\dot{r} = l + I_{yy}R_1 q + I_{yy}Q_1 r + I_{zx}Q_1 p + I_{zx}P_1 q - I_{zz}R_1 q - I_{zz}Q_1 r \quad (44)$$

$$I_{yy}\dot{q} = m - I_{xx}(P_1r + R_1p) + I_{xz}(2R_1r - 2P_1p) + I_{zz}(P_1r + R_1p) \quad (45)$$

$$I_{zz}\dot{r} - pI_{zx} = n + (Q_1p + P_1q)I_{xx} - (R_1q + Q_1r)I_{xz} - (Q_1p + P_1q)I_{yy} \quad (46)$$

$$p = \dot{\phi} - \dot{\Psi}_1\theta\cos(\Theta_1) - \dot{\psi}\sin(\Theta_1) \quad (47)$$

$$q = \dot{\Theta}_1\phi\sin(\Phi_1) + \dot{\phi}\cos(\Phi_1) + \dot{\Psi}_1\phi\cos(\Theta_1)\cos(\Phi_1) - \dot{\Psi}\theta\sin(\Theta_1)\sin(\Psi_1) + \dot{\psi}\cos(\Theta_1)\sin(\Phi_1) \quad (48)$$

$$r = -\dot{\Psi}_1\phi\cos(\Theta_1)\sin(\Phi_1) - \dot{\Psi}_1\theta\sin(\Theta_1)\cos(\Phi_1) + \dot{\psi}\cos(\Theta_1)\cos(\Phi_1) - \dot{\Theta}_1\phi\cos(\Phi_1) - \dot{\theta}\sin(\Phi_1) \quad (49)$$

Equations 41-49 are the perturbation equations of motion and perturbed kinematic equations. These equations can be further simplified by assuming that the aircraft is in straight, level, and rectilinear flight. This results in many steady-state values being zero.  $V_1 = W_1 = 0$  due to no side or upwards velocity.  $\Phi_1 = 0$  due to no initial bank angle.  $P_1 = Q_1 = R_1 = \Phi_1 = \Psi_1 = \dot{\theta}_1 = \dot{\Phi}_1 = 0$  because all angular rates are zero. These assumptions result in Equations 50-58.

$$m\dot{u} = f_x - mg\theta\cos(\Theta_1) \quad (50)$$

$$m\dot{v} = f_y + mg\phi\cos\Theta_1 - mU_1r \quad (51)$$

$$m\dot{w} = f_z - mg\theta\sin\Theta_1 + mU_1q \quad (52)$$

$$I_{xx}\dot{p} - I_{xz}\dot{r} = l \quad (53)$$

$$I_{yy}\dot{q} = m \quad (54)$$

$$I_{zz}\dot{r} - pI_{zx} = n \quad (55)$$

$$p = \dot{\phi} - \dot{\psi}\sin(\Theta_1) \quad (56)$$

$$q = \dot{\theta} \quad (57)$$

$$r = \phi\cos(\Theta_1) \quad (58)$$

Now that the perturbed equations of motion have been derived, the equations for the perturbed forces and moments need to be derived so they can be substituted into the perturbed equations of motion. This process will be illustrated for the perturbed force in the x-direction, followed by the resulting equations for all forces and moments.

First, all of the perturbations that have an effect on the force in the x direction need to be identified. These are state perturbations that alter the total force acting on the aircraft when the perturbations occur. The sum of all the perturbations is shown in 59.

$$f_x = \frac{\partial F_{A_x}}{\partial u}u + \frac{\partial F_{A_x}}{\partial q}q + \frac{\partial F_{A_x}}{\partial \alpha}\alpha + \frac{\partial F_{A_x}}{\partial \dot{\alpha}}\dot{\alpha} + \frac{\partial F_{A_x}}{\partial \delta_e}\delta_e + \frac{\partial F_{T_x}}{\partial u}u + \frac{\partial F_{T_x}}{\partial \alpha}\alpha \quad (59)$$

This is the dimensional quasi-steady model for perturbed forces in the x-direction, as shown in Roskam Figure 3.5 [6]. The A subscript is for aerodynamic forces, and the T subscript is for thrust forces. A quasi-steady model assumes that only one variable is changing at a time. This is the assumption that enables the calculation of the change in force in the x direction due to perturbations. To allow the force derivatives to be compared between different aircraft, the equation above needs to be non-dimensional as shown in equation 60.

$$f_x = \frac{\partial F_{A_x}}{\partial \frac{u}{U_1}}\frac{u}{U_1} + \frac{\partial F_{A_x}}{\partial \frac{q\bar{c}}{2U_1}}\frac{q\bar{c}}{2U_1} + \frac{\partial F_{A_x}}{\partial \alpha}\alpha + \frac{\partial F_{A_x}}{\partial \frac{\dot{\alpha}\bar{c}}{2U_1}}\frac{\dot{\alpha}\bar{c}}{2U_1} + \frac{\partial F_{A_x}}{\partial \delta_e}\delta_e + \frac{\partial F_{T_x}}{\partial \frac{u}{U_1}}\frac{u}{U_1} + \frac{\partial F_{T_x}}{\partial \alpha}\alpha \quad (60)$$

Each of these partial derivatives has a definition described in Chapter 3.2 of Roskam [6]. These definitions will be substituted into the equation, as shown in Equation 61.

$$f_x = \bar{q}_1 S ((-C_{D_u} + 2C_{D_l})\frac{u}{U_1} - C_{D_q}\frac{q\bar{c}}{2U_1} + \alpha(-C_{D_\alpha} + C_{L_l}) - C_{D_{\dot{\alpha}}}\frac{\dot{\alpha}\bar{c}}{2U_1} + C_{D_{\delta_e}}\delta_e + (-C_{T_{X_l}} + 2C_{T_{X_l}})\frac{u}{U_1}) \quad (61)$$

Most of the values in this equation are constants so the constant can be combined according to Table 5.1 from Roskam [6]. The constants that are formed are the longitudinal dimensional stability derivatives. It is assumed at this point that for trim flight:  $C_{Dq} = C_{D\alpha} = C_{T_{X_u}} = C_{T_{X_l}} = 0$ . The final equation for perturbed force in the x direction is Equation 62.

$$f_x = m(X_u u + X_\alpha \alpha + X_{\delta_e} \delta_e) \quad (62)$$

This equation can be substituted into the x-translational equation to get equation 63.

$$\dot{u} = X_u u + X_\alpha \alpha + X_{\delta_e} \delta_e - g \theta \cos(\Theta_1) \quad (63)$$

Repeat this process for the other perturbed forces and moments to get the equations 64-68.

$$\dot{v} = (Y_p p + Y_r r + Y_\beta \beta + Y_{\delta_a} \delta_a + Y_{\delta_r} \delta_r) + g \phi \cos \Theta_1 - U_1 r \quad (64)$$

$$\dot{w} - Z_\alpha \dot{\alpha} = (Z_u u + Z_\alpha \alpha + Z_q q + Z_{\delta_e} \delta_e) - g \theta \sin \Theta_1 + U_1 q \quad (65)$$

$$\dot{p} - \frac{I_{xz}}{I_{xx}} \dot{r} = L_p p + L_r r + L_\beta \beta + L_{\delta_a} \delta_a + L_{\delta_r} \delta_r \quad (66)$$

$$\dot{q} - M_\alpha \dot{\alpha} = (M_u u + M_\alpha \alpha + M_q q + M_{\delta_e} \delta_e) \quad (67)$$

$$\dot{r} - \frac{I_{xz}}{I_{zz}} \dot{p} = N_p p + N_r r + N_\beta \beta + N_{\delta_a} \delta_a + N_{\delta_r} \delta_r \quad (68)$$

These equations will be combined into a system of equations with Equations 63-68, with the  $\dot{\psi}$  term removed, as it does not affect the equations of motion. The equations are repeated below for clarity.

$$p = \dot{\phi}$$

$$q = \dot{\theta}$$

These eight linear equations will be combined to create the longitudinal and lateral models. The equations containing  $u, \alpha, q, \theta$  terms are combined to create the longitudinal model, and the equations containing  $p, \phi, \beta$ , and  $r$  terms are combined to create the lateral model.  $w$  and  $v$  are replaced with Equations 69 and 70. This allows the linear longitudinal and lateral state space model to be created which are Equation 13 and 14

$$w = U_1 \alpha \quad (69)$$

$$v = U_1 \beta \quad (70)$$

## Appendix B: System Transfer Functions

These equations were generated using the state space models and MATLAB code.

### A. Learjet 25 - Configuration 1 Lateral Transfer Functions

#### 1. Outputs with respect to Aileron Angle Input

$$\frac{v}{\delta_a} = \left( \frac{-1.722s^2 + 1.45s - 0.6825}{s^3 + 2.719s^2 + 3.817s + 7.645} \right) \left( \frac{-0.2235}{s + 0.000277} \right) \quad (71)$$

$$\frac{p}{\delta_a} = \left( \frac{-0.1464s^2 - 0.05711s - 0.498}{s^3 + 2.719s^2 + 3.817s + 7.645} \right) \left( \frac{0.0002038}{s + 0.000277} \right) \quad (72)$$

$$\frac{r}{\delta_a} = \left( \frac{-0.01106s^2 + 0.001199s - 0.02418}{s^3 + 2.719s^2 + 3.817s + 7.645} \right) \left( \frac{-0.004504}{s + 0.000277} \right) \quad (73)$$

$$\frac{\phi}{\delta_a} = \left( \frac{0.06018s^2 + 0.01703s + 0.189}{s^3 + 2.719s^2 + 3.817s + 7.645} \right) \left( \frac{-0.06036}{s + 0.000277} \right) \quad (74)$$

## 2. Outputs with respect to Rudder Angle Input

$$\frac{v}{\delta_r} = \left( \frac{0.02758s^2 + 0.4005s + 1.045}{s^3 + 2.719s^2 + 3.817s + 7.645} \right) \left( \frac{-0.113}{s + 0.000277} \right) \quad (75)$$

$$\frac{p}{\delta_r} = \left( \frac{0.002344s^2 + 0.03122s + 0.0819}{s^3 + 2.719s^2 + 3.817s + 7.645} \right) \left( \frac{0.0001031}{s + 0.000277} \right) \quad (76)$$

$$\frac{\beta}{\delta_r} = \left( \frac{0.0001771s^2 - 0.03517s - 0.08536}{s^3 + 2.719s^2 + 3.817s + 7.645} \right) \left( \frac{-0.002278}{s + 0.000277} \right) \quad (77)$$

$$\frac{\phi}{\delta_r} = \left( \frac{-0.0009638s^2 + 0.03123s + 0.07382}{s^3 + 2.719s^2 + 3.817s + 7.645} \right) \left( \frac{-0.03053}{s + 0.000277} \right) \quad (78)$$

,

## B. Learjet 25 - Configuration 1 Longitudinal Transfer Functions

### 1. Outputs with respect to Elevator Angle Input

$$\frac{u}{\delta_e} = \left( \frac{0.2432s - 0.002856}{s^2 + 3.086s + 12.3} \right) \left( \frac{-0.1723s + 0.6439}{s^2 + 0.006208s + 0.008397} \right) \quad (79)$$

$$\frac{w}{\delta_e} = \left( \frac{-1.242s - 83.03}{s^2 + 3.086s + 12.3} \right) \left( \frac{-0.001955s - 0.0006179}{s^2 + 0.006208s + 0.008397} \right) \quad (80)$$

$$\frac{q}{\delta_e} = \left( \frac{-0.1918s - 0.246}{s^2 + 3.086s + 12.3} \right) \left( \frac{0.0001171s + 0.0001679}{s^2 + 0.006208s + 0.008397} \right) \quad (81)$$

$$\frac{\theta}{\delta_e} = \left( \frac{0.02s - 0.1301}{s^2 + 3.086s + 12.3} \right) \left( \frac{-0.02s - 0.0002413}{s^2 + 0.006208s + 0.008397} \right) \quad (82)$$

### 2. Outputs with respect to Throttle Input

$$\frac{u}{\delta_T} = \left( \frac{4.616e^{-05}s - 2.998e^{-05}}{s^2 + 3.086s + 12.3} \right) \left( \frac{0.002243s + 7.306e^{-05}}{s^2 + 0.006208s + 0.008397} \right) \quad (83)$$

$$\frac{w}{\delta_T} = \left( \frac{-0.001051s - 0.01813}{s^2 + 3.086s + 12.3} \right) \left( \frac{-2.33e^{-06}s - 7.692e^{-09}}{s^2 + 0.006208s + 0.008397} \right) \quad (84)$$

$$\frac{q}{\delta_T} = \left( \frac{-3.884e^{-05}s - 3.102e^{-05}}{s^2 + 3.086s + 12.3} \right) \left( \frac{5.789e^{-07}s + 2.118e^{-08}}{s^2 + 0.006208s + 0.008397} \right) \quad (85)$$

$$\frac{\theta}{\delta_T} = \left( \frac{2.522e^{-06}s - 3.106e^{-05}}{s^2 + 3.086s + 12.3} \right) \left( \frac{2.522e^{-06}s + 5.633e^{-07}}{s^2 + 0.006208s + 0.008397} \right) \quad (86)$$

## Learjet 25 - Configuration 2 Lateral Transfer Functions

### 3. Outputs with respect to Aileron Angle Input

$$\frac{v}{\delta_a} = \left( \frac{1.318s - 0.9847}{s^2 + 0.2108s + 2.124} \right) \left( \frac{-1.339s - 0.2526}{s^2 + 1.156s - 0.02318} \right) \quad (87)$$

$$\frac{p}{\delta_a} = \left( \frac{-0.008231s - 0.003696}{s^2 + 0.2108s + 2.124} \right) \left( \frac{-0.06362s + 0.0002069}{s^2 + 1.156s - 0.02318} \right) \quad (88)$$

$$\frac{r}{\delta_a} = \left( \frac{0.002238s + 0.006199}{s^2 + 0.2108s + 2.124} \right) \left( \frac{-0.006013s - 0.004843}{s^2 + 1.156s - 0.02318} \right) \quad (89)$$

$$\frac{\phi}{\delta_a} = \left( \frac{0.001593s - 0.007783}{s^2 + 0.2108s + 2.124} \right) \left( \frac{-0.001593s - 0.06576}{s^2 + 1.156s - 0.02318} \right) \quad (90)$$

#### 4. Outputs with respect to Rudder Angle Input

$$\frac{v}{\delta_r} = \left( \frac{0.548s + 11.57}{s^2 + 0.2108s + 2.124} \right) \left( \frac{-0.3112s - 0.1487}{s^2 + 1.156s - 0.02318} \right) \quad (91)$$

$$\frac{p}{\delta_r} = \left( \frac{0.0281s - 0.04618}{s^2 + 0.2108s + 2.124} \right) \left( \frac{-0.0108s - 0.0003686}{s^2 + 1.156s - 0.02318} \right) \quad (92)$$

$$\frac{\beta}{\delta_r} = \left( \frac{-0.02427s - 0.001214}{s^2 + 0.2108s + 2.124} \right) \left( \frac{-0.00261s - 0.002702}{s^2 + 1.156s - 0.02318} \right) \quad (93)$$

$$\frac{\phi}{\delta_r} = \left( \frac{0.02177s + 0.03147}{s^2 + 0.2108s + 2.124} \right) \left( \frac{-0.02177s - 0.03609}{s^2 + 1.156s - 0.02318} \right) \quad (94)$$

### C. Learjet 25 - Configuration 2 Longitudinal Transfer Functions

#### 1. Outputs with respect to Elevator Angle Input

$$\frac{u}{\delta_e} = \left( \frac{0.2432s - 0.002856}{s^2 + 3.086s + 12.3} \right) \left( \frac{-0.1723s + 0.6439}{s^2 + 0.006208s + 0.008397} \right) \quad (95)$$

$$\frac{w}{\delta_e} = \left( \frac{-1.242s - 83.03}{s^2 + 3.086s + 12.3} \right) \left( \frac{-0.001955s - 0.0006179}{s^2 + 0.006208s + 0.008397} \right) \quad (96)$$

$$\frac{q}{\delta_e} = \left( \frac{-0.1918s - 0.246}{s^2 + 3.086s + 12.3} \right) \left( \frac{-0.0001171s + 0.0001679}{s^2 + 0.006208s + 0.008397} \right) \quad (97)$$

$$\frac{\theta}{\delta_e} = \left( \frac{0.02s - 0.1301}{s^2 + 3.086s + 12.3} \right) \left( \frac{-0.02s - 0.0002413}{s^2 + 0.006208s + 0.008397} \right) \quad (98)$$

#### 2. Outputs with respect to Throttle Input

$$\frac{u}{\delta_T} = \left( \frac{4.616e^{-05}s - 2.998e^{-05}}{s^2 + 3.086s + 12.3} \right) \left( \frac{0.002243s + 7.306e^{-05}}{s^2 + 0.006208s + 0.008397} \right) \quad (99)$$

$$\frac{w}{\delta_T} = \left( \frac{-0.001051s - 0.01813}{s^2 + 3.086s + 12.3} \right) \left( \frac{-2.33e^{-06}s - 7.692e^{-09}}{s^2 + 0.006208s + 0.008397} \right) \quad (100)$$

$$\frac{q}{\delta_T} = \left( \frac{-3.884e^{-05}s - 3.102e^{-05}}{s^2 + 3.086s + 12.3} \right) \left( \frac{5.789e^{-07}s + 2.118e^{-08}}{s^2 + 0.006208s + 0.008397} \right) \quad (101)$$

$$\frac{\theta}{\delta_T} = \left( \frac{2.522e^{-06}s - 3.106e^{-05}}{s^2 + 3.086s + 12.3} \right) \left( \frac{-2.522e^{-06}s + 5.633e^{-07}}{s^2 + 0.006208s + 0.008397} \right) \quad (102)$$

## D. F-4 Lateral Transfer Functions

### 1. Outputs with respect to Aileron Angle Input

$$\frac{p}{\delta_a} = \left( \frac{1.026s - 0.01685}{s^2 + 0.2297s + 5.74} \right) \left( \frac{8.747s + 5.15e^{-05}}{s^2 + 1.351s + 0.01755} \right) \quad (103)$$

$$\frac{\phi}{\delta_a} = \left( \frac{0.002936s + 1.027}{s^2 + 0.2297s + 5.74} \right) \left( \frac{-0.002936s + 8.743}{s^2 + 1.351s + 0.01755} \right) \quad (104)$$

$$\frac{\beta}{\delta_a} = \left( \frac{-0.0587s + 0.3007}{s^2 + 0.2297s + 5.74} \right) \left( \frac{0.05646s + 0.01447}{s^2 + 1.351s + 0.01755} \right) \quad (105)$$

$$\frac{r}{\delta_a} = \left( \frac{-0.3085s - 0.3278}{s^2 + 0.2297s + 5.74} \right) \left( \frac{0.05633s + 0.3205}{s^2 + 1.351s + 0.01755} \right) \quad (106)$$

### 2. Outputs with respect to Rudder Angle Input

$$\frac{p}{\delta_r} = \left( \frac{7.218s - 9.249}{s^2 + 0.2297s + 5.74} \right) \left( \frac{-5.492s + 0.02827}{s^2 + 1.351s + 0.01755} \right) \quad (107)$$

$$\frac{\phi}{\delta_r} = \left( \frac{1.611s + 7.588}{s^2 + 0.2297s + 5.74} \right) \left( \frac{-1.611s - 7.668}{s^2 + 1.351s + 0.01755} \right) \quad (108)$$

$$\frac{\beta}{\delta_r} = \left( \frac{0.0514s + 2.752}{s^2 + 0.2297s + 5.74} \right) \left( \frac{-0.03812s - 0.0125}{s^2 + 1.351s + 0.01755} \right) \quad (109)$$

$$\frac{r}{\delta_r} = \left( \frac{-2.686s + 0.3119}{s^2 + 0.2297s + 5.74} \right) \left( \frac{-0.09449s - 0.2809}{s^2 + 1.351s + 0.01755} \right) \quad (110)$$

## E. F-4 Longitudinal Transfer Functions

### 1. Outputs with respect to Elevator Angle Inputs

$$\frac{u}{\delta_e} = \left( \frac{-48.58s - 83.14}{s^2 + 1.258s + 8.106} \right) \left( \frac{60.83s + 22.08}{s^2 - 0.001006s - 0.001533} \right) \quad (111)$$

$$\frac{\alpha}{\delta_e} = \left( \frac{-0.03676s - 11.36}{s^2 + 1.258s + 8.106} \right) \left( \frac{-0.01909s - 0.007234}{s^2 - 0.001006s - 0.001533} \right) \quad (112)$$

$$\frac{q}{\delta_e} = \left( \frac{-11.37s - 5.744}{s^2 + 1.258s + 8.106} \right) \left( \frac{-0.01089s - 0.001086}{s^2 - 0.001006s - 0.001533} \right) \quad (113)$$

$$\frac{\theta}{\delta_e} = \left( \frac{0.7086s - 10.48}{s^2 + 1.258s + 8.106} \right) \left( \frac{-0.7086s - 0.01017}{s^2 - 0.001006s - 0.001533} \right) \quad (114)$$

## Appendix C: Bode Plots

### F. F-4 Bode plots

The plots were produced using MATLAB and are too numerous to put into the main body of the document, and

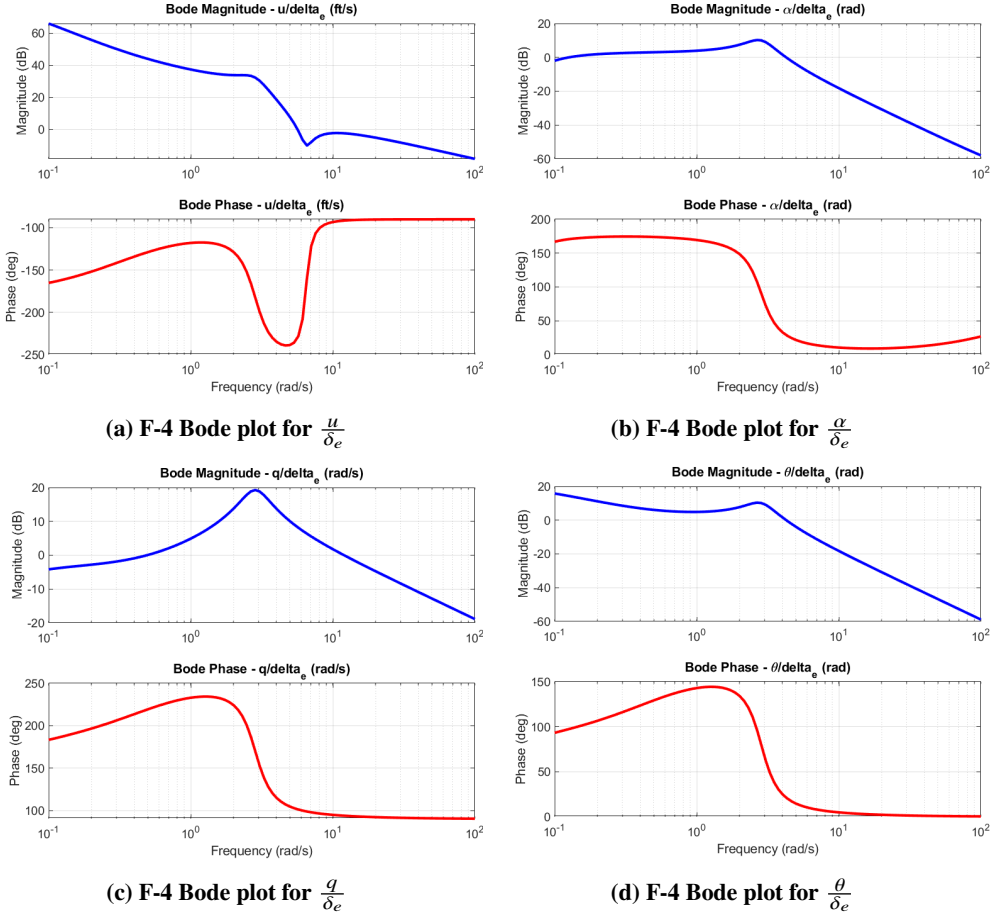


**Fig. 41 Longitudinal Bode Plots For F-4**

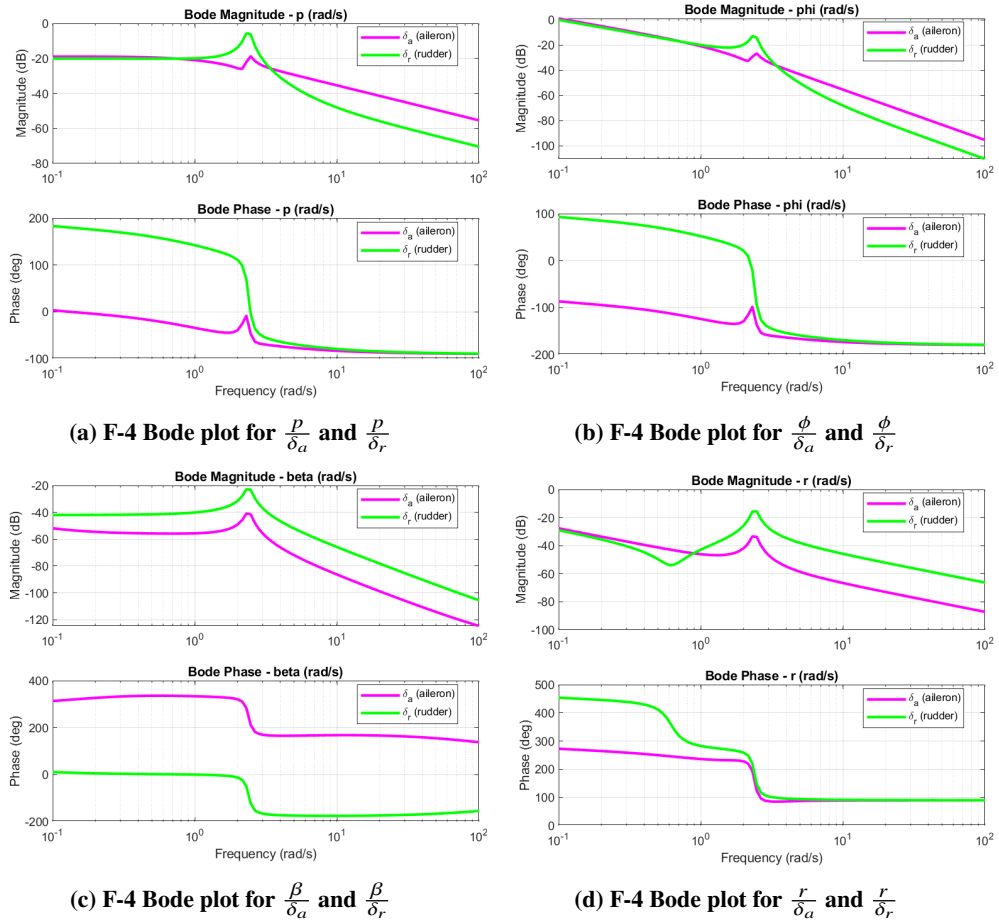


**Fig. 42 Lateral Bode Plots For F-4**

## G. Learjet-25 Configuration 1 Bode plots

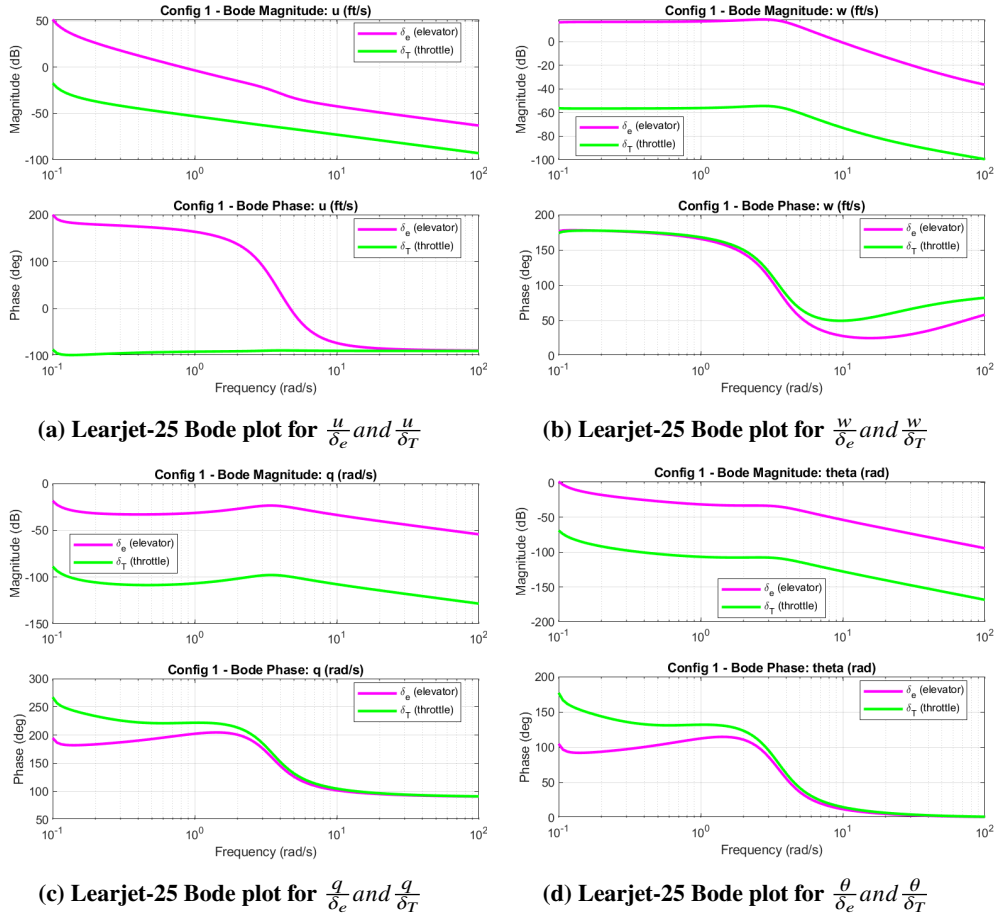


**Fig. 43 Longitudinal Bode Plots For Learjet-25 Configuration 1**

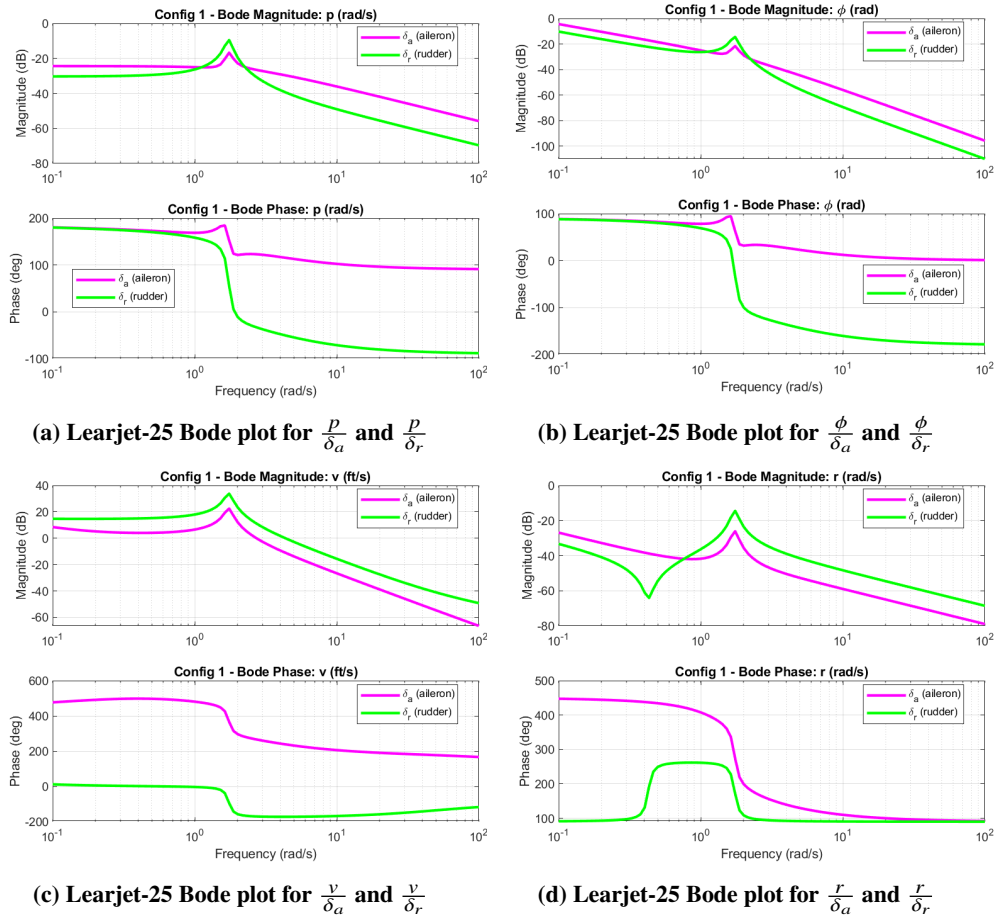


**Fig. 44 Lateral Bode Plots For Learjet-25 Configuration 1**

## H. Learjet-25 Configuration 2 Bode plots

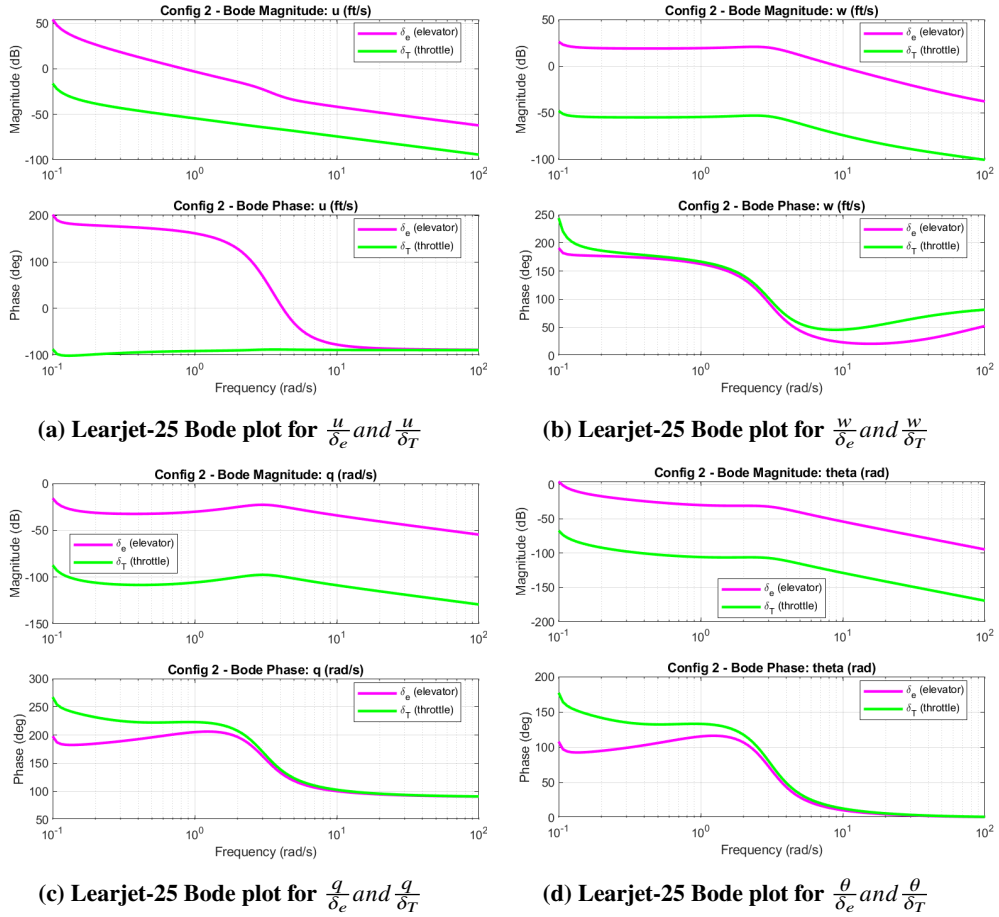


**Fig. 45 Longitudinal Bode Plots For Learjet-25 Configuration 2**

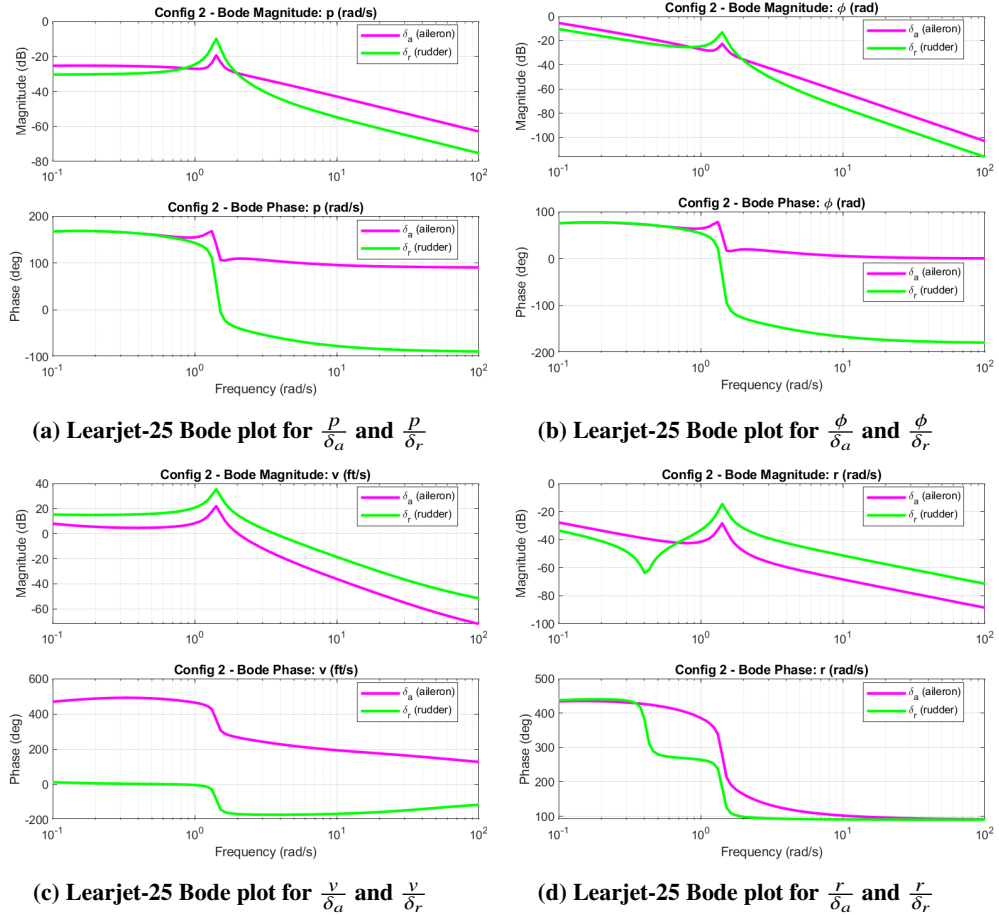


**Fig. 46 Lateral Bode Plots For Learjet-25 Configuration 2**

## Appendix D: Individual contributions

- Abstract
- Nomenclature
- Introduction and Conclusion
- F-4 nonlinear system
- Nonlinear to linear derivation/Appendix A
- F-4 linear system
- Model validation
- Learjet-25 linear systems
- Handling Qualities
- Transfer Functions and Frequency Responses
- Simulator
- Controllers
- Elevator Failure analysis
- Appendix B
- Appendix C
- Editor
- Ethan Wegner
- Jacob Hansen
- Ethan Wegner
- Jacob Hansen
- Jacob Hansen
- Laynie Aure and Paige Ward
- Ethan Wegner
- Kaylee Patterson, Nate Jacobs, and Paige Ward
- Carissa Castellano
- Kaylee Patterson and Nate Jacobs
- Tiger Sievers
- Tiger Sievers
- Paige Ward
- Kaylee Patterson and Paige Ward
- Jacob with provided bode plots from Kaylee Patterson and Nate Jacobs
- Laynie Aure and Tiger Sievers

## References

- [1] Randall Beard and Timothy W. McLain. *Small Unmanned Aircraft: Theory and Practice*. Princeton University Press, 2012.
- [2] John Burken Curtis Hanson Nhan Nguyen. *Handling Qualities Evaluations of Low Complexity Model Reference Adaptive Controllers for Reduced Pitch and Roll Damping Scenarios*. Tech. rep. August 11, 2011. URL: <https://ntrs.nasa.gov/api/citations/20110023802/downloads/20110023802.pdf>.
- [3] Donald W. Gallagher David L. Green Hal Andrews. *Interpreted Cooper-Harper for broader use*. Tech. rep. NASA. Ames Research Center, Piloting Vertical Flight Aircraft: A Conference on Flying Qualities and Human Factors, September 1, 1993. URL: <https://ntrs.nasa.gov/citations/19940008836>.
- [4] Immanuel Barshi Jeb S. Orr Irving C Statler. *The X-15 3-65 Accident: An Aircraft Systems and Flight Control Perspective*. Tech. rep. NASA Ames Research Center, Space and Saftey is no Accident Conference, October 20, 2014. URL: <https://ntrs.nasa.gov/citations/20190001985>.
- [5] David Peahl. “A Survey of Handling Qualities Criteria and their Applications to High Performance Aircraft”. PhD thesis. California Polytechnic State University, 1986.
- [6] Jan Roskam. *Airplane Flight Dynamics and Automatic Controls Part 1*. DAR Corp., 2001.
- [7] Flight Standards Service. *Airplane Flying Handbook*. U.S Department of Transportation: Federal Aviation Administration, 2021. URL: [https://www.faa.gov/sites/faa.gov/files/regulations\\_policies/handbooks\\_manuals/aviation/airplane\\_handbook/00\\_afh\\_full.pdf](https://www.faa.gov/sites/faa.gov/files/regulations_policies/handbooks_manuals/aviation/airplane_handbook/00_afh_full.pdf).
- [8] Mark B. Tischler Tom Berger. “Identification of a Full-Envelope Learjet-25 Simulation Model Using a Stitching Architecture”. In: *Journal of Guidance, Control, and Dynamics* 43.11 (2020), pp. 2091–2111. doi: 10.2514/1.G005094. URL: <https://arc.aiaa.org/doi/10.2514/6.2015-1594>.